Climate Data Record (CDR) Program

Climate Algorithm Theoretical Basis Document (C-ATBD)

MSU/AMSU Radiance Fundamental Climate Data Record Calibrated Using Simultaneous Nadir Overpasses

CDR Program Document Number: CDRP-0015
Originator Document Number: TBD
Version 1.0 / February, 2012

RESPONSIBILITY

Prepared By:	Cheng-Zhi Zou Wenhui Wang	Physical Scientist Scientist	NOAA/NESDIS I.M. Systems Group
	Signature		Date
Reviewed By:	<Name>	<Title>	<Organization>
	Signature		Date
Reviewed By:	<Name>	<Title>	<Organization>
	Signature		Date
Approved By:	<Name>	<Title>	<Organization>
	Signature		Date
Approved By:	<Name>	<Title>	<Organization>
	Signature		Date

REVISION HISTORY

Version	Description	Revised Sections	Date
1.0	Initial submission to CDR Program	New Document	02/27/2012

TABLE of CONTENTS

LIST OF FIGURES

LIST OF TABLES

ACRONYMS AND ABBREVIATIONS

Acronym or Abbreviation	Meaning
AMSU	Advanced Microwave Sounding Unit
AMSU-A	Advanced Microwave Sounding Unit-A
ATBD	Algorithm Theoretical Basis Document
BT	Brightness Temperature
CATBD	Climate Algorithm Theoretical Basis Document
CDR	Climate Data Record
CDRP	Climate Data Record Program
CHAMP	CHAllenging Minisatellite Payload
CFSR	Climate Forecast System Reanalysis
COSMIC	Constellation Observing System for Meteorology Ionosphere & Climate
ECMWF	European Centre for Medium-Range Weather Forecast
EOS	Earth Observing System
EUMETSAT	European Meteorological Satellite Agency
FCDR	Fundamental Climate Data Record
FOV	Field of View
GPS	Global Positioning System
GRACE	Gravity Recovery And Climate Experiment
IFOV	Instantaneous Field of View
IR	Infrared
JPSS	Joint Polar Satellite System
LEO	Low Earth Orbit
LZA	Local Zenith Angle
MERRA	Modern Era Retrospective-analysis for Research and Applications
MetOp-A	European Meteorological Operational satellite programme
MSU	Microwave Sounding Unit
NASA	National Aeronautics and Space Administration
NCDC	National Climatic Data Center
NESDIS	National Environmental Satellite, Data, and Information Service
NCEP	National Centers for Environmental Prediction

NeDT	Noise Equivalent Difference of Temperature
NIR	Near Infrared
NOAA	National Oceanic and Atmospheres Administration
NPOESS	National Polar-orbiting Operational Environmental Satellite System
NWP	Numerical Weather Prediction
PRT	Platinum Resistance Thermometer
RAOB	Radiosonde Observation
RMSE	Root Mean Square Error
RO	Radio Occultation
SAC-C	Satellite de Aplicaciones Cientificas-C
SNO	Simultaneous Nadir Overpass
STAR	Center for Satellite Applications and Research
TCDR	Thematic Climate Data Record
TOVS	TIROS Operational Vertical Sounder

1. Introduction

1.1 Purpose

The purpose of this document is to describe the algorithm submitted to the National Climatic Data Center (NCDC) by Cheng-Zhi Zou at NOAA/NESDIS/Center for Satellite Applications and Research that will be used to create the radiance Fundamental Climate Data Record (FCDR), using the Microwave Sounding Unit (MSU) and Advanced Microwave Sounding Unit-A (AMSU-A). The actual algorithm is defined by the computer program (code) that accompanies this document, and thus the intent here is to provide a guide to understanding that algorithm, from both a scientific perspective and in order to assist a software engineer performing an evaluation of the code.

1.2 Definitions

Following is a summary of the symbols used to define the algorithm.

MSU/AMSU level-1c calibration equation and parameters:

$$R = R_L - \delta R + \mu Z \tag{1-1}$$

where

R = *Earth scene radiance*

$R_L = R_c + S(C_e - C_c)$ = *Earth scene radiance from the linear calibration*

$Z = S^2(C_e - C_c)(C_e - C_w)$ = *Non- linear response*

$S = \dfrac{R_w - R_c}{C_w - C_c}$ =*Slope determined by the space cold and onboard blackbody warm calibration targets*

R_w =*Radiance of the onboard blackbody warm target*

R_c = *Radiance of the cosmic space cold target*

C_e = *Raw counts data of the Earth scene*

C_w = *Raw counts data of the warm target view*

C_c = *Raw counts data of the cold target (cosmic space) view*

δR= *Calibration offset (determined by post-launch calibration)*

μ= Non-linear calibration coefficient (determined by post-launch calibration)

Supplemental simultaneous nadir overpass (SNO) regression algorithm for obtaining calibration coefficients:

$$\Delta R = \Delta R_L - \Delta\delta R + \mu_k Z_k - \mu_j Z_j \quad (1\text{-}2)$$

where

$$\Delta R = R_k - R_j$$

$$\Delta R_L = R_{L,k} - R_{L,j}$$

$$\Delta\delta R = \delta R_k - \delta R_j$$

k and j = satellite index referring to satellites k and j, respectively

Z_k and Z_j = Non-linear responses for satellites k and j, respectively

μ_k, and μ_j = Non-linear coefficients for satellites k and j, respectively

Equation 1-1 provides the level-1c radiance FCDR with given variables from observations except for δR and μ. The regression algorithm (Equation 1-2) obtains values of three calibration coefficients, $\Delta\delta R$, μ_k, and μ_j using SNOs with a strong constraint that the instrument temperature variability in the calibrated radiances is minimal. A sequential procedure is then applied to obtain calibration coefficients for all recalibrated satellite channels. Equation 1-1 is the main algorithm for the data processing described in this document. Equation 1-2 is an offline supplement to Equation 1-1 which helps the readers to understand how the calibration coefficients are obtained. Equation 1-2 is not part of the processing code described in this document. Details on how to solve for the calibration coefficients are described in the Algorithm Section.

1.3 Document Maintenance

The algorithm has been used to inter-calibrate all atmospheric temperature sounding channels of MSU/AMSU-A instruments. The main products of the algorithm are calibration coefficients and their resulting radiance FCDR datasets. Two changes may occur to the algorithm and its resulting datasets: major changes to the theoretical basis of the calibration algorithm and update of the resulting calibration coefficients and their associated FCDR dataset. The first change is not expected to occur frequently since the calibration theory and equations are fairly mature. However, if a change does occur, the document will be rewritten to include the new theory and results.

The second change is expected to occur more frequently. This is because satellite observations inter-calibrated before need to be recalibrated in a routine (e.g. yearly) basis when new observations such as those from the Advanced Technology Microwave Sounder (ATMS) onboard National Polar-orbiting Operational Environmental Satellite System (NPOESS) Preparatory Project (NPP) and to be flown on Joint Polar Satellite System (JPSS) are available. Recalibration will provide updated calibration coefficients and radiance FCDR datasets that include new satellite observations. These updates will be documented as supplements to this document. After a substantial set of satellite channels are recalibrated, version update for the document will be provided to include results of the newly inter-calibrated satellite channels.

2. Observing Systems Overview

This section provides an overview of characteristics of the MSU/AMSU observing systems and its calibration strategy. It also describes radiance FCDR requirements and characteristics generated by the MSU/AMSU-A inter-calibration algorithm.

2.1 Products Generated

The SNO inter-calibration algorithm generates swath level-1c radiance data at each scan position on the MSU/AMSU-A scan-lines. The MSU and AMSU-A have respectively 11 and 30 field of views (FOVs) on each scan-line. Table 2-1 and

Table 2-2 respectively list the requirements and characteristics for the radiance MSU and AMSU-A FCDR datasets derived from the SNO inter-calibration.

Table 2-1 Requirements on the radiance FCDR from the MSU Observations. Due to a linear relationship between the radiances and brightness temperatures in the microwave soundings, the requirements are provided with respect to the brightness temperature measurements.

Radiance FCDRs from MSU	**Requirement**
Product Geographic Coverage/Conditions	Global coverage except heavy precipitation
Product Vertical Resolution (km)	Radiance products represent atmospheric layer temperatures; Vertical resolution represented by channel weighting functions is 3 to 5 km
Product Horizontal Resolution (km)	110 km at nadir to 320 km at limb
Product Measurement Range (K)	180 K– 320 K
Product Absolute Calibration Accuracy (K) (relative to assumed SI-Traceable Standards)	1K

Product Relative Calibration Accuracy (K) (relative to the same MSU measurement but onboard different satellites)	Operational Calibration: 1K SNO Inter-Calibration: 0.1-0.2K
Product Refresh Rate/Coverage Time	Global coverage: 1 day
Product length	28 years (Nov. 1978-Sep. 2006)
Step time per measurement	1.84 seconds
Product Calibration Precision (K)	0.03-0.05 K in global mean for SNO calibration; 0.15-0.20K in global mean for operational calibration

Table 2-2 Same as Table 2-1 except for AMSU-A instrument.

Radiance FCDRs from AMSU	**Requirement**
Product Geographic Coverage/Conditions	Global coverage except heavy precipitation
Product Vertical Resolution (km)	Radiance products represent atmospheric layer temperatures; Vertical resolution represented by channel weighting functions is 1 to 3 km
Product Horizontal Resolution (km)	45 km at nadir
Product Measurement Range (K)	180 – 320K
Product Absolute Calibration Accuracy (K) (relative to assumed SI-Traceable Standard)	0.5-1K
Product Relative Calibration Accuracy (K) (relative to the same AMSU measurement but onboard different satellites)	Operational Calibration: 0.5-1K SNO Inter-Calibration: 0.1-0.2K
Product Refresh Rate/Coverage Time	Global coverage: 1 day
Product length	13 years (Oct. 1998-present)
Step time per measurement	0.2 seconds
Product Calibration Precision (K)	0.03-0.05 K in global mean for SNO calibration

2.2 Instrument Characteristics

MSU and AMSU-A are both cross-track, line-scanned instruments designed to measure Earth scene radiances. The detailed system parameters and measurement principles for MSU and AMSU-A can be found in Kidwell (e.g., 1998) and Robel et al. (2009). Here only the instrument characteristics related to the SNO inter-calibration and FCDR development are briefly described.

2.2.1 MSU

MSU is a microwave Dicke radiometer with four-channels to make passive measurements in the 5.5 millimeter oxygen region. The four channels respond to the following respective spectral frequencies: 50.3, 53.74, 54.96, and 57.95 GHz with a channel bandwidth of 200 MHz in each case, and a typical NEΔT of 0.3K. The MSU sensors consist of two four-inch diameter antennas named as MSU-1 and MSU-2, respectively. Each of the two antennas has an IFOV of 7.5 degrees. The MSU-1 is used by channels 1 and 2 while MSU-2 by channels 3 and 4. The antennas are step-scanned through eleven individual 1.84-second Earth viewing steps and require a total of 25.6 seconds to complete.

The MSU instrument uses an on-board calibration method that includes two calibration targets as its end point references: the cosmic space cold target and an onboard blackbody warm target. The cold space has a temperature of 2.73 K, and the warm target temperature is measured by the platinum resistance thermometers (PRT) embedded in the blackbody target. There are 2 PRTs embedded on the blackbody target. The antennas view the cold target and the warm target once during each scan cycle. The signals from the Earth views and target views in the form of electric voltage are converted to digital counts through an analog-to-digital converter, which are output as the raw observations. The MSU level-1c calibration converts the raw counts data of the 11 Earth views to radiances using the one cold and one warm target views as references in each scan-line.

The MSU instrument parameters can be found in Kidwell (1998) and are also summarized in Table 2-3.

Table 2-3 MSU instrument parameters.

Cross-track scan angle (degrees from nadir)	± 47.35
Scan time (seconds)	25.6
Number of steps	11
Angular FOV (degrees)	7.5
Step angle (degrees)	9.47
Step time (seconds)	1.84

Ground IFOV at nadir (km diameter)	109.3
Ground IFOV at end of scan	323.1 km cross-track x 178.8 km along-track
Distance between IFOV centers (km along-track)	168.1 km
Swath width	± 1174 km
Time between start of each scan line	25.6 sec
Step and dwell time	1.81 sec
Time difference between the start of each scan and the center of the first dwell period	0.9 sec
Total Channels	4
Channel Frequencies (GHz)	CHs: 1 2 3 4 Frequency: 50.30 53.74 54.96 57.95
Instrument Antenna Systems	MSU-1 and MSU-2
Responsible antennas for each channel	MSU-1 for channels 1 and 2 MSU-2 for channels 3 and 4
Channel Bandwidth (MHz)	200
Blackbody and space views per scan line	1
PRTs on each warm target	2

2.2.2 AMSU-A

As a successor to the MSU instrument, the AMSU-A has 15 discrete frequency channels to measure the Earth scene radiances. At each channel frequency, the antenna beamwidth is a constant of 3.3 degrees (at the half power point). Thirty contiguous scene resolution cells are sampled in a stepped-scan fashion (i.e., the instrument's FOV rotates to a data collection position, stops, collects data, then moves to the next collection position, stops, collects data, etc.) every eight seconds, each scan covering 48.33 degrees on each side of the nadir direction. The AMSU-A instrument starts at earth position 1, then goes sequentially to earth position 30, then to the cold calibration view position and then to the warm load view position. These scan patterns and geometric resolution translate to a 45 km diameter cell at nadir and a 2,343 km swath width from the 833 km nominal orbital altitude. Detailed AMSU-A instrument characteristics can be found in the NOAA KLM user's guide (Robel et al., 2009)

AMSU-A has two units: A1 and A2; where A1 has two antenna systems, A1-1 and A1-2, and A2 has its own antenna system. Channels 6-7 and 9-15 use A1-1 antenna system, channels 3-5 and 8 use A1-2 antenna system, and channels 1-2 use A2

antenna system. There is a blackbody warm target for each anntana system. Each scan-line contains 30 Earth views, two space views, and two warm target views. The PRTs on each target ranges from 5 to 7, depending on instrument subunits. The averages of the two space views or blackbody views are used to calibrate the 30 Earth views. The warm target temperature is the average of the available good PRTs measurements for each instrument.

Table 2-4 and Table 2-5 summarize the AMSU-A instrument parameters.

Table 2-4 AMSU-A instrument parameters.

Cross-track scan angle (degrees from nadir)	± 48.33
Earth Scene scan time	5.965 seconds
Total Beam Positions	30
Angular FOV (degrees)	3.33
Step angle (degrees)	3.33
Step time (seconds)	0.1988
Ground IFOV at nadir (km diameter)	50km
Swath width	± 1171 km
Time between start of each scan line	8 sec
Step and dwell time	0.1988 sec

Table 2-5 Channel and scanning view parameters for each AMSU-A antenna systems.

Instrument Antenna systems	**A1-1**	**A1-2**	**A2**
Channels	6-7,9-15	3-5, 8	1-2
Earth views per scan line	30	30	30
Blackbody and space views per scan line	2	2	2
PRTs in each warm target	5	5	7

3. Algorithm Description

This section describes the MSU/AMSU-A radiance FCDR algorithms at 80% level of maturity. The MSU/AMSU-A FCDR contains pixel radiances at each scan position in the scan-lines with the original beam directions as well as the limb-corrected beam directions. Only level-1c calibration algorithm is described.

3.1 Algorithm Overview

The MSU/AMSU-A radiance FCDR is developed using the simultaneous nadir overpass (SNO) calibration method (Zou et al., 2006, 2009; Zou and Wang, 2010, 2011). The SNO method inter-calibrates the level-1c (root-level) MSU and AMSU-A observations by determining offsets and non-linear calibration coefficients from SNO matchups. The SNO method takes advantages that the SNO matchups do not contain sampling errors such as the diurnal drift errors, so the statistical differences in the SNO matchups represent only instrument calibration errors in the satellite pairs. The method removed or minimized four types of inter-satellite biases, including relatively stable inter-satellite biases between most satellite pairs, bias drifts on NOAA-16 and certain channels on MetOp-A, sun-heating induced instrument temperature variability in satellite radiances, scene temperature dependency in biases due to inaccurate calibration non-linearity. The inter-calibration resulted in consistent, nearly identical multi-satellite observations. In addition, SNO analysis method was developed to identify post-launch channel frequency shift from pre-launch specifications or measurements. Using radiative transfer model experiments at the SNO sites, actual channel frequency values were obtained for certain AMSU-A channels. These corrected frequencies are expected to improve accuracies of future applications of these channels in Numerical Weather Prediction (NWP) data assimilation, climate reanalysis development, as well as TCDR time series development.

3.2 Processing Outline

The MSU and AMSU-A radiance FCDR production systems are designed and implemented separately due to differences in instrument characteristics and computer software applied. However, the processing outlines for the two instruments are similar, which are described using the same flowchart as seen below. There is a note for each flowchart to indicate the differences between the MSU and AMSU-A processing systems if such differences exist.

3.2.1 Overall Processing Outline

The overall processing outline of MSU/AMSU-A radiance FCDR algorithm is summarized in Figure 3-1. The current MSU/AMSU-A FCDR algorithm is implemented at orbital-level, with one inter-calibrated level-1c file corresponding to one MSU/AMSU-A level-1b file. In an orbit, Earth view raw counts data are converted to radiances scan-line by scan-line. Limb-corrected radiances are also generated to adjust off-nadir observations to nadir equivalent observations.

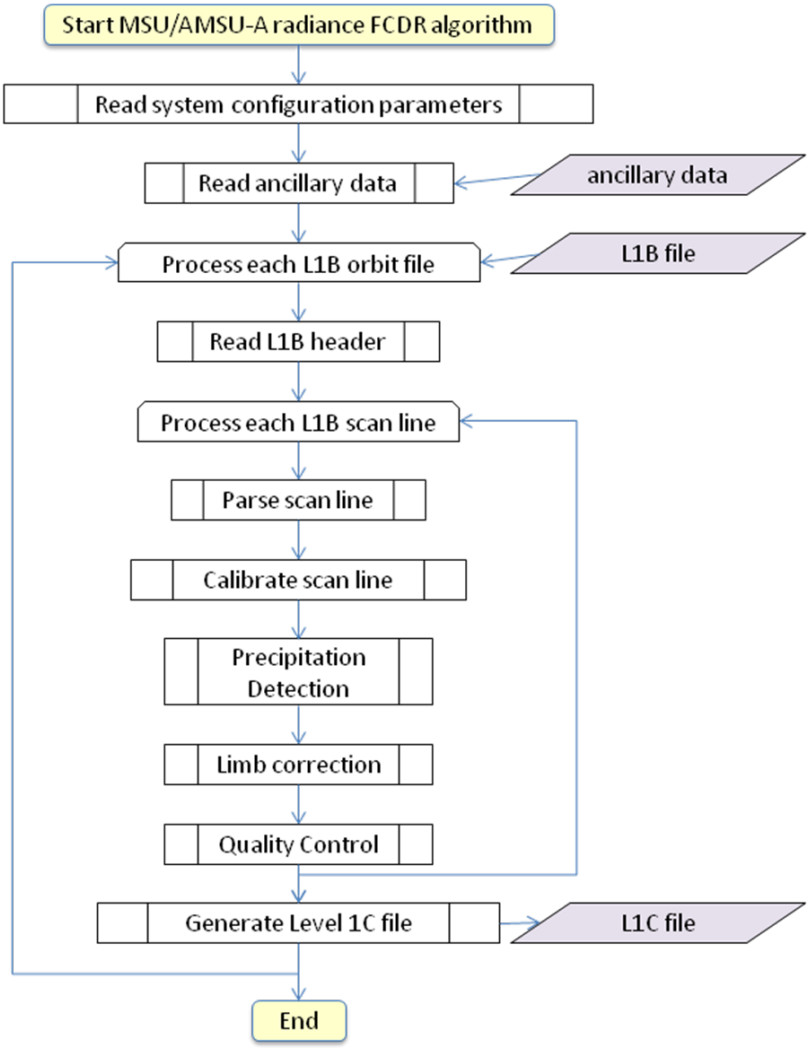

Figure 3-1 High level flowchart of the MSU/AMSU-A FCDR algorithm illustrating the main processing section.

3.2.2 System configuration

The processing starts with system configuration, including defining satellite names, level-1b input and level-1c output directories, ancillary data directories, and calibration methodologies (Figure 3-2). In addition to the SNO inter-calibration method, the FCDR production system supports two other calibration methods: the NOAA pre-launch calibration and linear calibration. The AMSU-A FCDR generation system supports parallel processing to address the large data volume issue in AMSU-A. System operators should first define the maximum number of the level-1b files that can be simultaneously processed by the computer based on the computer hardware environment.

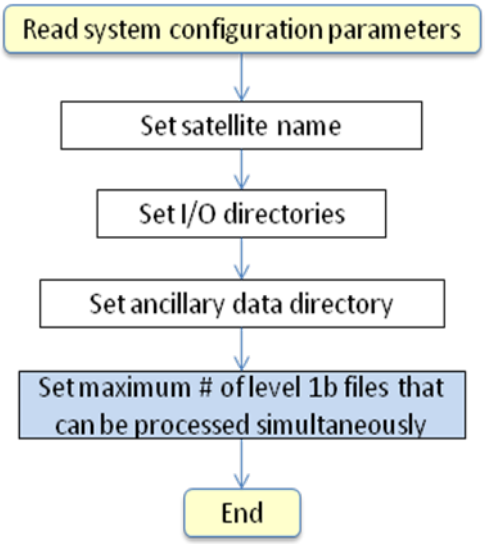

Figure 3-2 Input parameter processing flowchart for the MSU/AMSU-A FCDR. The box with light blue background is for AMUS-A only. Note: the MSU code doesn't support parallel processing.

3.2.3 Preparing Ancillary Data

Several ancillary data are required to generate level-1c recalibrated files from level-1b files. These ancillary data consist of land fraction, SNO calibration coefficients, and limb correction coefficients. Figure 3-3 shows the flowchart for preparing the ancillary data. Note that the antenna pattern correction coefficients are not available for the MSU observations, so the 'read antenna pattern correction coefficients' component should be removed for the MSU processing system. In addition, the AMSU-A antenna pattern correction is not currently used for all satellites.

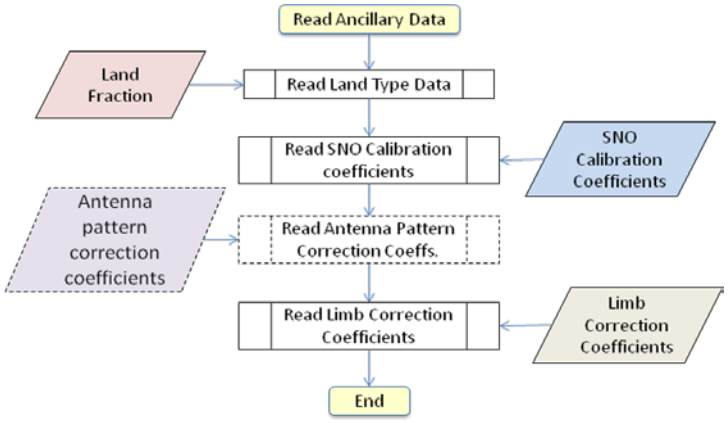

Figure 3-3 AMSU-A FCDR flowchart for preparing the ancillary data. There is no antenna pattern correction for the MSU instrument; therefore, the 'read antenna pattern correction coefficients' component should be removed when the flowchart is used for the MSU processing system.

3.2.4 Processing Level-1b Header Record

The header record in each MSU/AMSU-A level-1b file contains orbit-wide information for the subsequent calibration process. These information include data creation site ID, satellite/instrument ID, observation time, number of data record, instrument reference temperature, warm target and cold space correction factors (AMSU-A only), central wave numbers (AMSU-A only), coefficients for calculating nonlinear parameters, coefficients for converting raw counts of varies instrument temperature readings to the actual instrument temperatures, etc. Figure 3-4 illustrates how AMSU-A header record is processed in the FCDR processing system. The MSU systems have less parameters than the AMSU-A for processing.

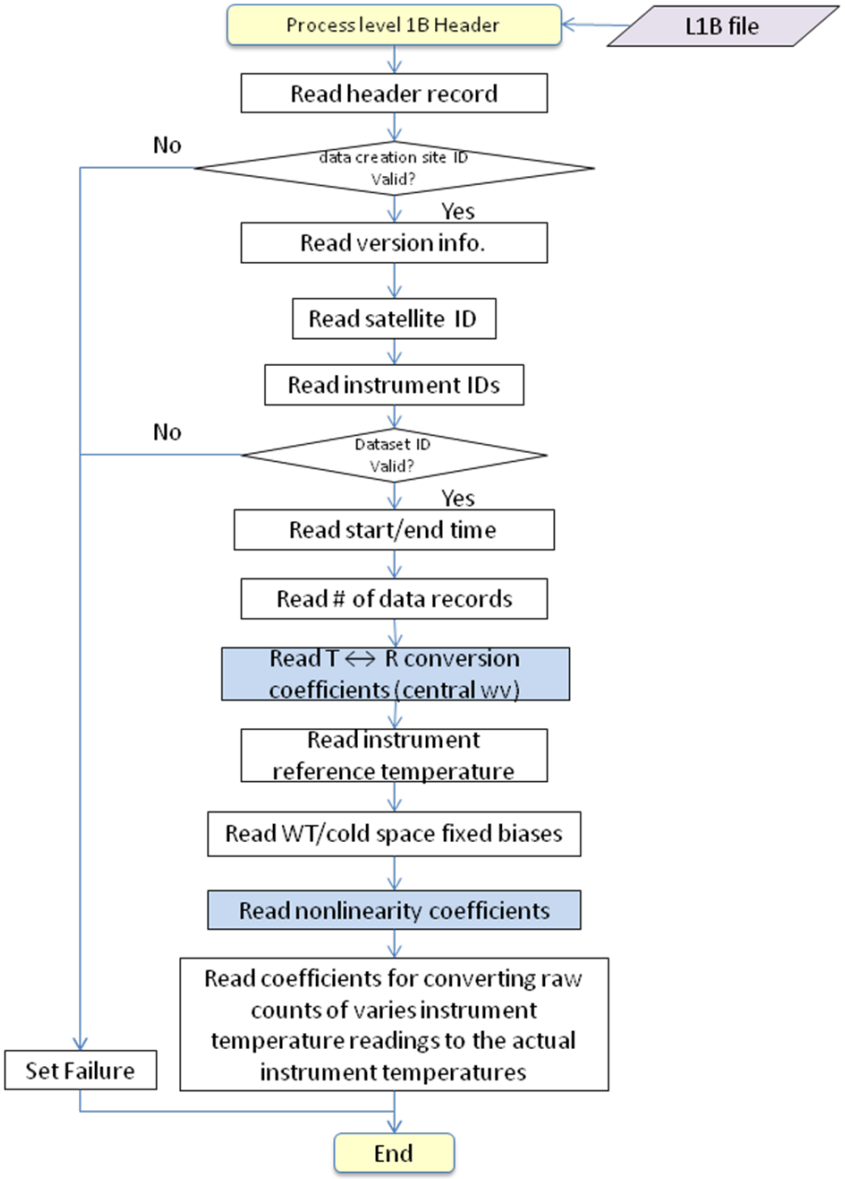

Figure 3-4 Flowchart for processing MSU/AMSU-A level 1B header record (steps with light blue background are for AMSU-A only).

3.2.5 Preprocessing Level-1b Scan Line

Each level-1b file is decoded line by line before generating a level-1c scan line. Figure 3-5 shows flowchart for preprocessing each AMSU-A level-1b data record.

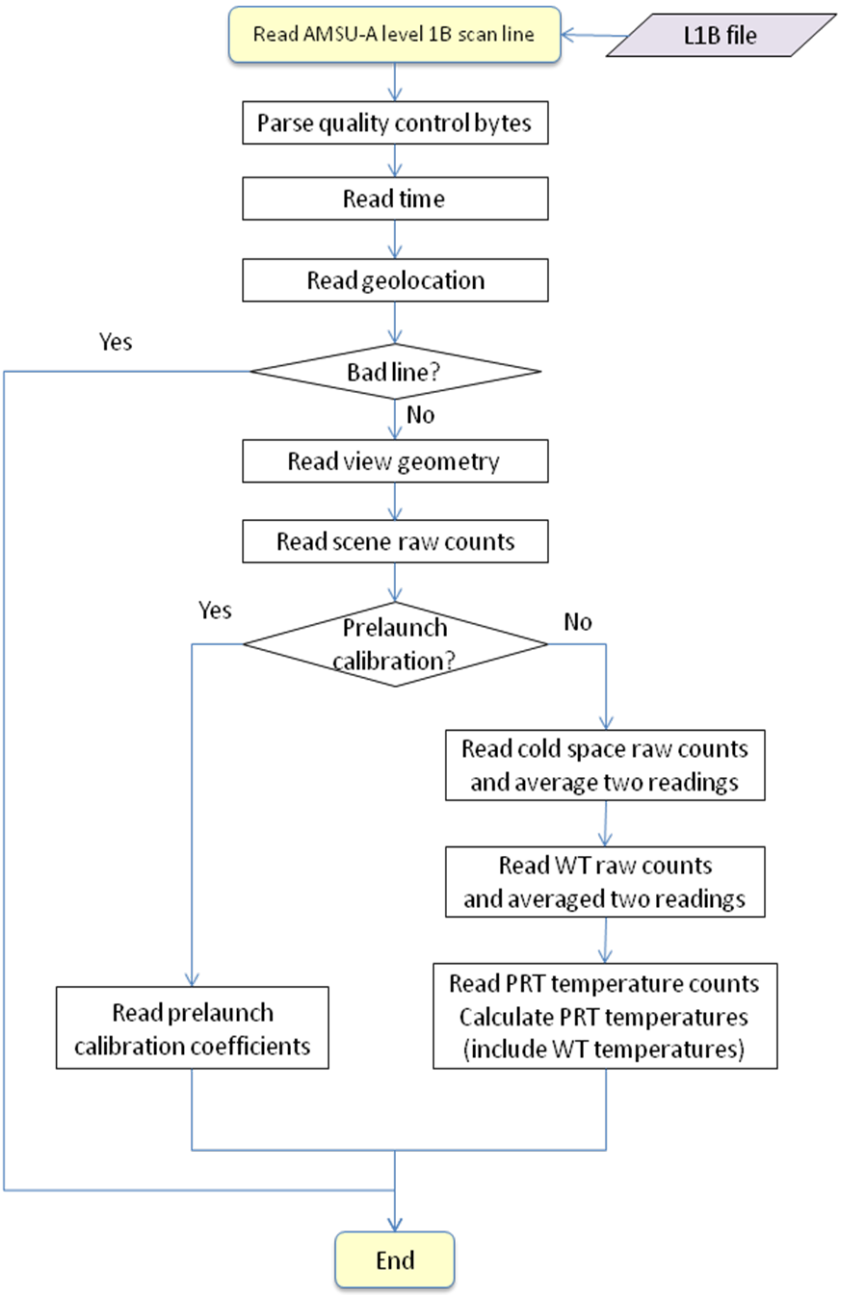

Figure 3-5 Flowchart of parse MSU/AMSU-A FCDR level-1b scan line.

3.2.6 Level-1c Calibration

Figure 3-6 shows the flowchart of the level 1c calibration process for converting the Earth scene raw counts to radiances. There are three calibration methodologies in the processing system: SNO, pre-launch, and linear calibrations. The FCDR outputs contain calibrated radiances from both the SNO and pre-launch calibrations for channels with available SNO calibration coefficients (MSU channels 2-4, AMSU-A channels 4-14). For channels without the SNO calibration coefficients (MSU channel 1, AMSU-A channels 1-3, 15), only prelaunch operational calibration is conducted. The linear calibration is optional in the processing system for research purposes—its output is not part of the FCDR dataset.

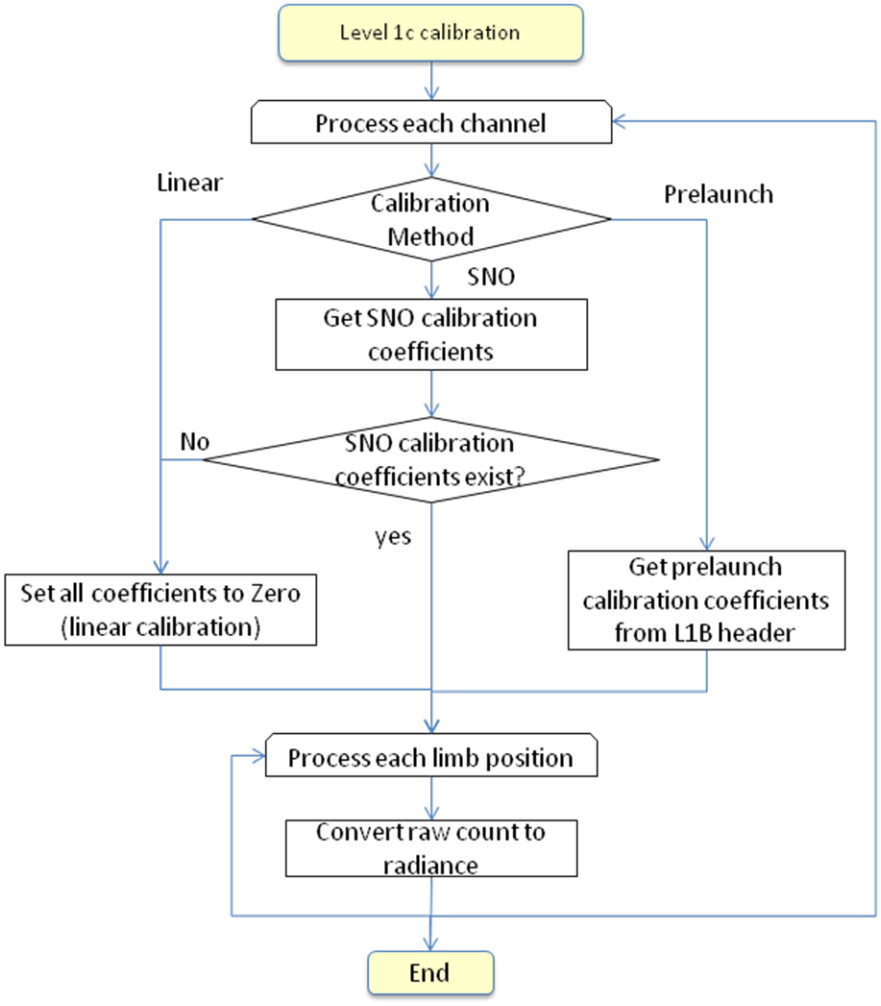

Figure 3-6 Flowchart of the MSU/AMSU-A level-1c calibration.

3.3 Algorithm Input

This section describes the attributes of all input data used by the algorithm, including primary sensor data and ancillary data.

3.3.1 Primary Sensor Data

Table 3-1 lists the primary sensor data (data directly available from the MSU/AMSU-A level-1b files used by the MSU/AMSU-A FCDR algorithm, including raw counts for the Earth scene view, warm target view, and cold space view; warm target temperatures, geo-location information, and sensor quality flags).

Table 3-1. MSU/AMSU-A primary sensor data at pixel level. The dimension 'xsize' is the pixel number per scan-line (11 for MSU and 30 for AMSU-A) and 'ysize' is the total scan-line number in an orbital file.

Name	Type	Description	Dimension
Earth Scene Raw Counts	Input	Earth Scene raw counts for atmospheric temperature channels (MSU channels 1-4; AMSU-A channels 1-15)	pixel (xsize, ysize)
Cold Space Raw Counts	Input	Cold Space raw counts corresponding to each MSU/AMSU-A atmospheric temperature channel	pixel (xsize, ysize)
Warm target raw Counts	Input	Warm target raw counts corresponding to each MSU/AMSU-A atmospheric temperature channel	pixel (xsize, ysize)
Warm target temperatures	Input	Warm target temperatures, average of the available good PRT readings	pixel (xsize, ysize)
Latitude	Input	Pixel center latitude	pixel (xsize, ysize)
Longitude	Input	Pixel center longitude	pixel (xsize, ysize)
QC flags	Input	quality control flags from level-1b data	pixel (xsize, ysize)
Pre-launch calibration coefficients	Input	Pre-launch calibration coefficients	

The actual sensor inputs are different for different calibration methods. The SNO and linear calibrations require the raw counts data for the Earth scene, cold space view, and warm target view, as well as the warm target temperatures. The NOAA pre-launch calibration takes a simplified form where the Earth scene radiance is polynomial proportional to the Earth scene counts with the raw counts and temperatures for the calibration targets as well as the nonlinear coefficients of the original calibration

equation being absorbed in the calibration coefficients of the polynomial equation. See Section 3.4 for a theoretical description of the SNO calibration method and the NOAA KLM Users Guide (Robel et al., 2009) for the NOAA pre-launch calibration method.

3.3.2 Ancillary Data

The calibration algorithm requires three types of ancillary data:

i. SNO inter-calibration coefficients (Table 3.2 for MSU and Table 3.3 for AMSU-A);

ii. Limb correction coefficients (available in the FCDR generation system package);

iii. Land type data [land or ocean, where a pixel is considered as ocean (land) if the ocean percentage in the pixel is greater (smaller) than 50%]

3.3.3 Derived Data

Not Applicable.

3.3.4 Forward Models

Not applicable.

3.4 Theoretical Description

This section describes the physics on the development of consistent MSU/AMSU radiance FCDR using SNO inter-calibration algorithm. There are two parts in the algorithm:

(i) obtain the calibration coefficients using the regression equation 1-2.

(ii) calculate consistent radiance FCDR data using the calibration equation 1-1.

The second part of calculation is straightforward given the sensor data from the level-1b files and the ancillary data described in Section 3.3.2. It is similar to the operational calibration except the latter uses calibration coefficients determined from laboratory chamber test experiments (e.g., Mo, 2006) while the former uses calibration coefficients determined by SNO regressions of Equation 1-2. This part of the algorithm mainly involves data processing similar to operational calibration and its physical basis has been well established in documents describing the operational level-1b data processing (e.g., Mo, 2006; Robel et al., 2009, and related references). However, results of the part (i) algorithm are a prerequisite for deriving the radiance FCDR using the part (ii) algorithm and the part (i) algorithm itself involves a good understanding of the calibration errors, SNO regressions, and a comprehensive end-to-end calibration

process to determine the calibration coefficients as listed in Tables 3-2 and 3-3. In the following sections, part (ii) algorithm is described first (Section 3.4.1) followed by a description of the part (i) algorithm (Section 3.4.2). Part (i) can be skipped if one is only interested in generating the final radiance FCDR products using the given calibration coefficients.

3.4.1 Physical and Mathematical Description

The MSU and AMSU instruments use an on-board calibration method that includes two calibration targets as its end point references: the cosmic space cold target and an onboard blackbody warm target. The cold space has a temperature of 2.73 K, and the warm target temperature is measured by the platinum resistance thermometers (PRT) embedded in the blackbody target. In each scan cycle, the MSU/AMSU-A looked at these targets as well as the earth, and the signals in the form of electric voltage were converted to digital counts through an analog-to-digital converter. These digital counts were output as raw observations. A calibration equation, also known as radiometer transfer function, is used to converting the raw counts observations to the radiances using the two calibration targets.

The level-1c calibration equation to generate the MSU/AMSU-A FCDR is written as (Zou et al., 2006, 2009):

$$R = R_L - \delta R + \mu Z \qquad (3\text{-}1)$$

where R is the earth scene radiance, $R_L = R_c + S(C_e - C_c)$, representing the dominant linear response, and $Z = S^2(C_e - C_c)(C_e - C_w)$ is a nonlinear response. C represents the raw counts data of the satellite observations and $S = \frac{R_w - R_c}{C_w - C_c}$ is the slope determined by the two calibration targets. The subscripts *e, w* and *c* refer to the earth-view, onboard blackbody warm target view, and cold space view, respectively; δR represents a radiance offset; and μ is a nonlinear coefficient. A schematic viewing of this calibration process is illustrated in Figure 3-7.

In Equation 3-1, the cold space radiance R_c is set to be the value that corresponds to a brightness temperature of 4.73 K for all scan lines of the MSU and AMSU observations. This value includes the cold-space temperature of 2.73 K plus an increase of about 2 K owing to the antenna side-lobe radiation. The algorithms described in (Kidwell, 1998) for MSU and in (Robel et al., 2009) for AMSU are used to compute R_w. Once the offset, δR, and the nonlinear coefficient, μ, are known, radiance is computed through Equation 3-1 and the brightness temperature, T_b, is then computed using the Planck function.

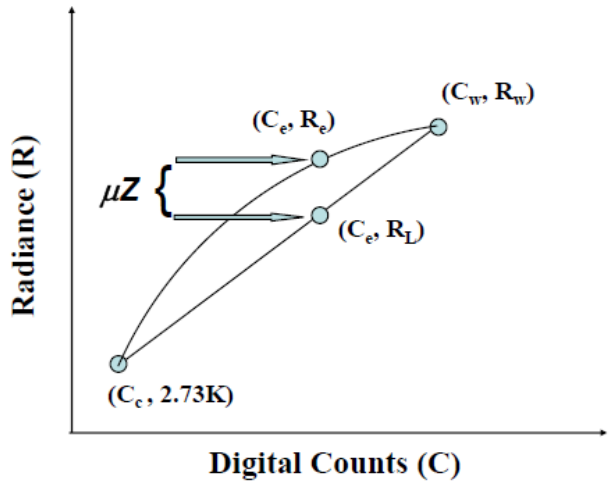

Figure 3-7 Schematic viewing the calibration principle of the MSU/AMSU instruments. Symbols used in the plot are defined in the main text.

Equation 3-1 or 1-1 is a modified version of the algorithm used by NOAA for operational generation of the level-1c products, where δR was assumed to be zero and the non-linear coefficient μ was determined from pre-launch laboratory tests (Mo, 1996). These coefficients have been converted to polynomial coefficients with respect to scene counts (Robel et al., 2009) and then stored in AMSU-A level 1b files. Radiances calculated using coefficients in AMSU-A level 1b files are hence referred to as the operational calibration. However, because this procedure was repeated for each AMSU-A instrument independently, it was not designed to correct for residual biases between satellites.

In the inter-satellite calibration described in this document, the offset δR in Equation 3-1 allows for removal of inter-satellite differences. In addition, the calibration coefficients, δR and μ, were determined using SNO matchups. There is another difference from the operational calibration. In specific, the raw counts values of the calibration targets in Equation 3-1 were averages over 7 adjacent scan lines in the operational calibration (Mo, 1996). However, in the SNO inter-satellite calibration, target counts values of a single scan line were used to calibrate each Earth scene observation in that scan line. This change was made because SNOs are collected for individual near nadir footprints. When deriving calibration coefficients from SNOs, target observations closest to the SNO footprints, which are those from the same scan lines of the SNO events, are used to eliminate potential non-simultaneous errors. Limited experiments indicate that this change may increase the noise in the level-1c radiances by 2% compared to those using the original method of averaging adjacent scan lines. This small extra noise is not expected to affect the quality of the resulting level-1c radiances. However, if future evidence suggests that this will cause large errors in the weather and climate reanalysis data assimilations, we will use the operational algorithm for target counts calculation but with SNO calibration coefficients applied.

Quality control procedure in the operational calibration is used in the SNO inter-calibration to deal with missing calibration information, instrument anomalies, and bad scan lines.

3.4.2 Inter-Satellite Calibration Methodology

Developing consistent radiance FCDR mainly involves minimizing inter-satellite radiance biases between satellite pairs through an inter-calibration process. A SNO inter-calibration methodology is developed at NOAA/NESDIS (Zou et al., 2006, 2009) to remove or minimize calibration errors that were not well resolved by the pre-launch operational calibration processes. These errors include relatively stable inter-satellite biases between most satellite pairs, bias drifts in certain satellite channels, sun-heating induced instrument temperature variability in radiances, scene temperature dependency in biases due to inaccurate calibration non-linearity, and biases owing to channel frequency shift from its prelaunch measurement in certain satellite channels. A detailed description on the origin and nature of these biases can be found in Zou and Wang (2011).

Optimal calibration coefficients, δR and μ, were determined from SNO repressions to remove the first four types of biases. The SNO matchups, occurring mostly over the Polar Region around 80°S and 80°N, were accumulated using Cao et al.'s (2004) algorithm. The ground distance and time criteria for the SNO matchups were respectively set to be 111 km and 100 seconds for the MSU satellites for TIROS-N through NOAA-14 and 45 km and 50 seconds for the AMSU-A satellites for NOAA-15 through NOAA-18, and MetOp-A. The SNO matchups do not contain sampling errors such as the diurnal drift errors. Therefore, the statistical differences in the SNO matchups represent instrument calibration errors in the satellite pairs.

Applying the calibration Equation 3-1 to the SNO matchups between two satellites, represented by *k* and *j*, a radiance error between them is derived as,

$$\Delta R = \Delta R_L - \Delta\delta R + \mu_k Z_k - \mu_j Z_j + E \qquad (3\text{-}2)$$

where $\Delta R_L = R_{L,k} - R_{L,j}$ and $\Delta\delta R = \delta R_k - \delta R_j$. *E* is a residual term related to the spatial and time differences between the satellites *k* and *j* and is ignored. In Equation 3-2, ΔR_L, Z_k and Z_j are a function of the measurements while $\Delta\delta R$, μ_k, and μ_j are unknown coefficients. Regression methods are used to solve for these coefficients from the SNOs in which the summation of $(\Delta R)^2$ is minimized. Optimum values of the three parameters, $\Delta\delta R$, the difference between μ_k and μ_j, (μ_k-μ_j), and the absolute values of μ_k or μ_j, determined from the regressions remove three different type of errors: the mean radiance bias in the satellite pair, the scene temperature dependency in biases, and the sun-heating induced instrument temperature variability in the radiances.

Figure 3-8 shows an example of the brightness temperature differences in the SNO matchups between NOAA-10 and NOAA-11 before and after applications of the

SNO regression coefficients in the calibration Equation 3-1. In specific, Figure 3-8a shows SNO scatter plot between NOAA-10 and NOAA-11 of the linear calibrated MSU channel 2 observations. Inter-satellite bias of -0.3 K and scene temperature dependency in the biases are clearly seen in the plot. These biases occur due to inaccurate offsets and calibration nonlinearity. These scene temperature dependent biases can be quantified by the slope of the SNO scatter plot between the two satellites. This slope (0.0206) results in about 0.3 K biases between NOAA-11 and NOAA-10 for a temperature range of 150 K (from 200 to 250K). This scene temperature dependency causes the inter-satellite biases to depend on the latitudinal zones as well as seasons.

Figure 3-8b shows the same SNO scatter plot but with brightness temperatures being calculated from applying the optimum calibration coefficients determined from the SNO regressions. It is clearly seen that the SNO determined calibration coefficients have removed the mean inter-satellite biases in the satellite pairs and significantly reduced the scene temperature dependency in the biases.

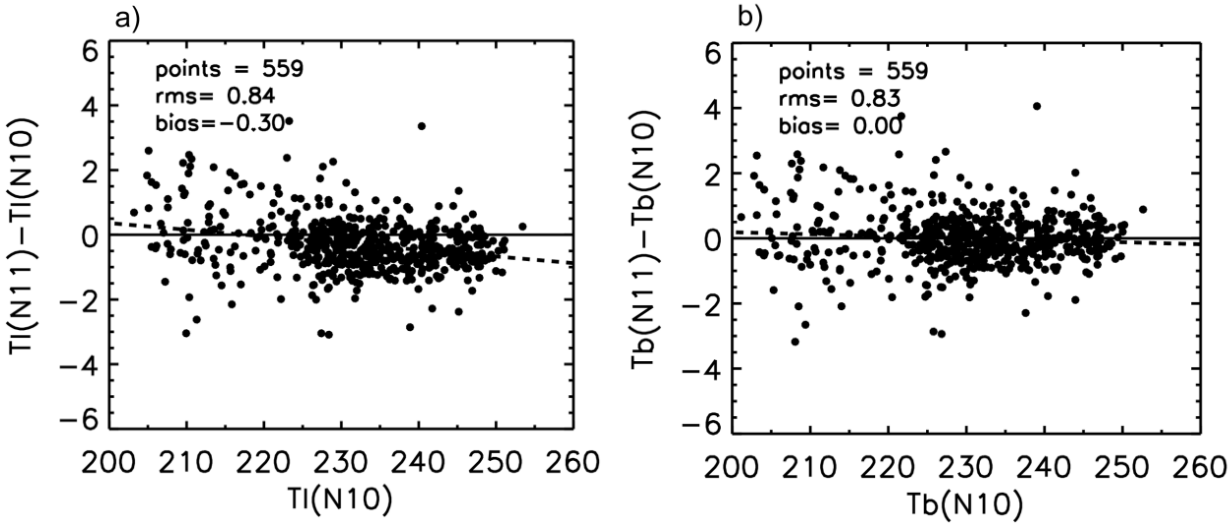

Figure 3-8 (a) SNO scatter plot between T_b(N10) and δT_b = T_b(N11)-T_b(N10), showing scene temperature dependent biases when T_b (represented by T_L) is obtained by linear calibration equation. The regression linear fitting (dashed lines) is expressed as ΔT_L = 4.491–0.0206×T_L(N10); (b) Same as (a) but for SNO calibrated data between T_b(N10) and δT_b = T_b(N11)-T_b(N10). The regression linear fitting (dashed lines) is expressed as ΔT_b = 1.42–0.00615×T_b(N10) (Plots from Zou et al. 2006).

Note that optimum differences of the calibration coefficients, $\Delta\delta R$ and (μ_k-μ_j), are sufficient to remove the inter-satellite biases and their scene temperature dependency in Figure 3-8. Thus the absolute values of the calibration coefficients must be determined using other information. For this purpose, one of the satellites in the pair (*k* and *j*) should be selected as a reference satellite. For this reference satellite, the calibration offset needs to be determined from an absolute calibration or validation processes against observations from other reference observations. Since such

references do not exist, the offset of the reference satellite is arbitrarily chosen to be zero.

The absolute value of the nonlinear coefficient of the reference satellite is determined using the requirement that instrument temperature dependency in the radiances must be minimal for the satellite pair. Using NOAA-15 and NOAA-16 satellite pair as an example, Figure 3-9 visually demonstrates how absolute values of optimum calibration coefficients were obtained from the SNO calibration procedure. In the plot, the quadratic curves in each panel respectively represent calibration equations for NOAA-15 and NOAA-16 for a specific combination of the non-linear coefficients, μ_{N15} and μ_{N16}, with their differences, μ_{N15}-μ_{N16}, determined by their SNO matchups. Also shown in each panel is their SNO T_b difference time series corresponding to the calibration curves within the panel. Changing the calibration coefficient, μ_{N15}, of the reference satellite also changes μ_{N16} due to their SNO constraint. These changes resulted in graduate changes in magnitude from Figures 3-9a to 3-9d of the sun-heating induced instrument temperature variability in their SNO T_b difference time series. Only a unique combination of the calibration coefficients μ_{N15} and μ_{N16} minimizes the instrument temperature variability (Figure 3-9c). For a more detailed description of the procedure, the readers are referred to Zou et a**l.** (2006, 2009) and Zou and Wang (2011).

Based on these SNO regression characteristics, a sequential procedure (Zou et al., 2006, 2009) was developed to obtain calibration coefficients for the MSU/AMSU-A instruments for all satellites. Following this method, a reference satellite is selected and its calibration coefficients, δR and μ, are assumed to be known temporarily. Then calibration coefficients of all other satellites are determined sequentially (one by one) from regressions of the SNO matchups between satellite pairs, starting from the satellite closest to the reference satellite. For the MSU observations, NOAA-10 was selected to be the reference satellite. For AMSU-A observations, the reference satellites were selected to be NOAA-18 for channel 6 and NOAA-15 for all other channels. The calibration offset δR was arbitrarily set to be zero for the reference satellite since it does not affect the climate variability and trends. The sequential procedure actually reduces the problem to the determination of the nonlinear coefficient of the reference satellite; since once it is known, calibration coefficients of all other satellites are solved from the SNOs.

The nonlinear coefficient of the reference satellite was determined by the requirement that the averaged sun heating induced temperature variability in the radiances for all satellite pairs should be minimal. To meet this requirement, a series of sensitivity experiments was conducted in which the nonlinear coefficient of the reference satellite was selected at different values within a reasonable range. For each given value, a set of calibration coefficients for all other satellites were obtained sequentially from regressions of the SNO matchups. For each set of calibration coefficients, level-1c radiances were generated for all satellites and the sun heating induced temperature variability were examined in the global ocean mean time series. The final determination of the nonlinear coefficient was made when the average of this

variability is minimal for all satellites. This approach generates a set of level-1c radiances that does not depend on the initial selection of the reference satellite. Figure 3-10 shows the flowchart for the above described sequential procedure.

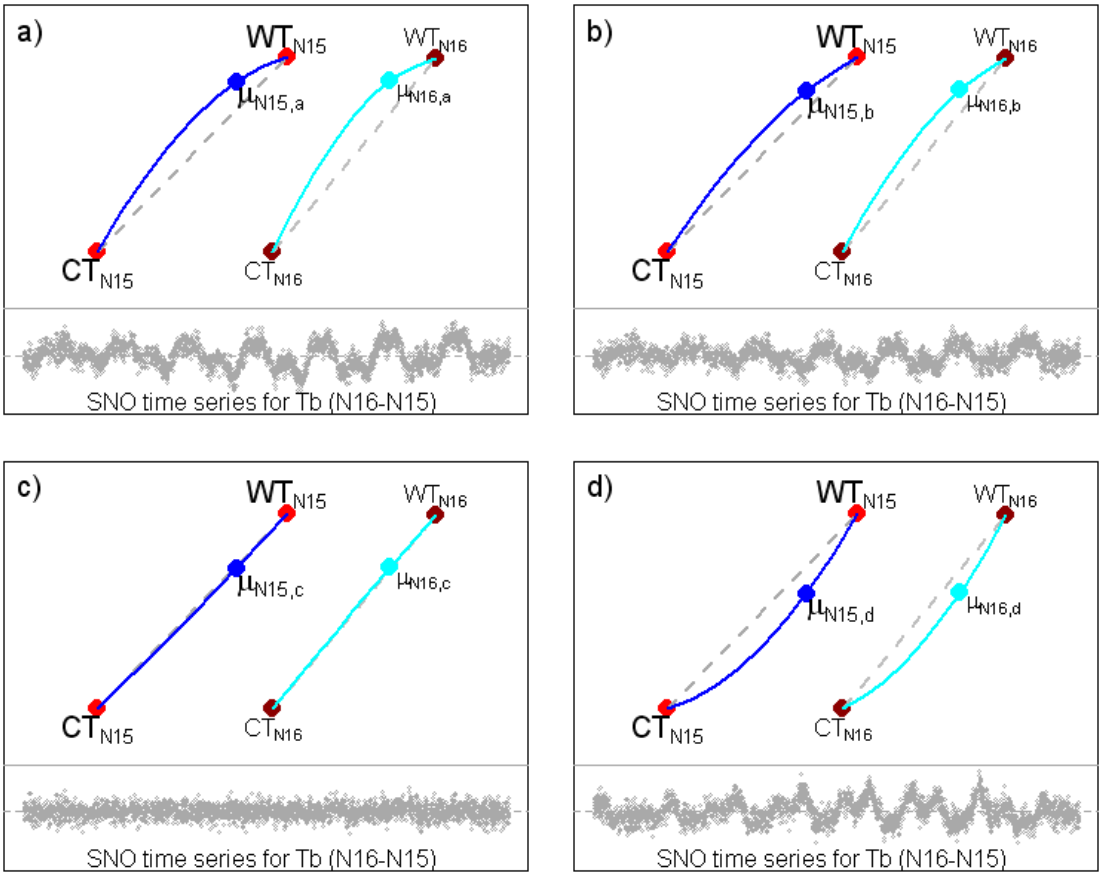

Figure 3-9 Schematic plots showing how sun-heating-induced instrument temperature signals in radiances were removed by appropriate combination of the non-linear calibration coefficients between two satellites. In each panel, the top two quadratic curves respectively represent calibration equations for NOAA-15 and NOAA-16 corresponding to different values of non-linear coefficients μ_{N15} and $\mu_{N16,}$ where the horizontal coordinate represent the raw counts and the vertical coordinate represents the radiance. Symbols CT and WT stand for cold and warm targets, respectively. The lower time series are SNO T_b differences for channel 7 between the two satellites (NOAA-16 minus NOAA-15) with horizontal coordinates being the time and vertical coordinates being the T_b differences. Note the graduate changing of the sun-heating-induced instrument temperature variability in the SNO time series for panels (a), (b), (c) and (d). Also note only at a unique combination of μ_{N15} and μ_{N16} (panel c) that this instrument temperature variability is mostly removed.

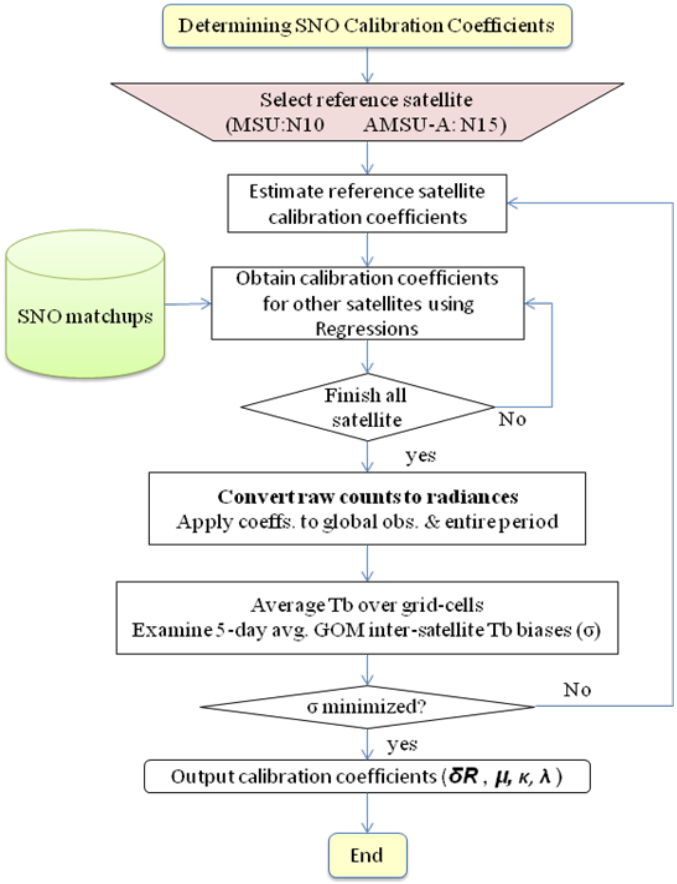

Figure 3-10 Sequential procedure for determining MSU/AMSU-A calibration coefficients.

3.4.2.1 The MSU Calibration Coefficients

By design, the sequential method minimizes inter-satellite biases, scene temperature dependency in biases, and the sun-heating induced instrument temperature variability in the radiances. In the MSU case, optimal constant calibration coefficients were obtained for all satellites (Zou et al., 2009). Table 3-2 lists these calibration coefficients. Figure 3-11 demonstrates the performance of these coefficients by showing global ocean-mean inter-satellite brightness temperature difference time series of prelaunch calibration (Figure 3-11a) compared to those obtained from the SNO calibration coefficients in Table 3-2 (Figure 3-11b). As seen, inter-satellite biases and the sun heating induced instrument variability as observed in Figure 3-11a for NOAA-10 through NOAA-14 are mostly removed in Figure 3-11b. In addition, scene temperature dependency in biases were also significantly reduced (Figure 3-8)

Table 3-2 Calibration coefficients for MSU channels 2, 3, and 4 for different satellites obtained from the SNO sequential procedure, where δR is the offset and μ the nonlinear coefficient. Units for δR and μ are 10^{-5} (mW) (sr m^2 cm^{-1}) $^{-1}$ and (sr m^2 cm^{-1}) $(mW)^{-1}$, respectively.

Satellite	Channel 2		Channel 3		Channel 4	
	δR	**μ**	***δR***	**μ**	***δR***	**μ**
NOAA TIROS-N	1.3963	5.4062	5.7535	1.2941	1.6808	4.8256
NOAA 6	0	7.3750	0.1162	6.1974	-1.5438	6.5032
NOAA 7	0	7.4380	-2.8131	10.4644	-1.9660	6.5637
NOAA 8	-1.3750	8.2636	1.4737	4.4531	-0.5083	5.5242
NOAA 9	-0.0771	5.9713	0.1026	9.0332	0.7721	6.1028
NOAA 10	0	6.2500	0	5.6300	0	4.9500
NOAA 11	-2.4641	9.5909	-1.9983	7.1892	-0.7271	5.4574
NOAA 12	-0.0996	6.7706	-2.3979	8.3282	-4.6074	7.1040
NOAA 14	-0.6363	7.4695	-3.0810	8.7524	-0.7753	5.4175

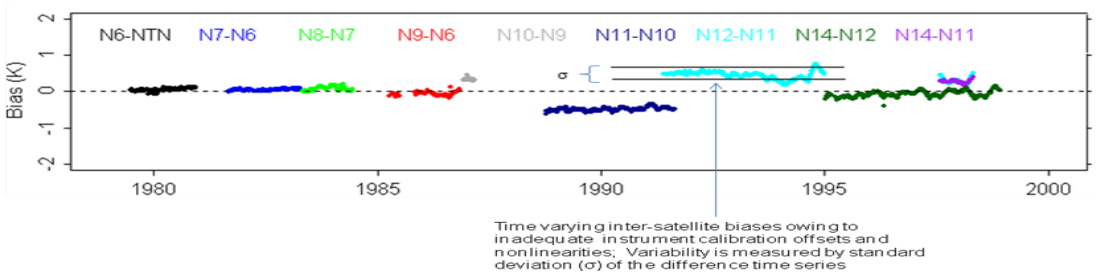

(a)

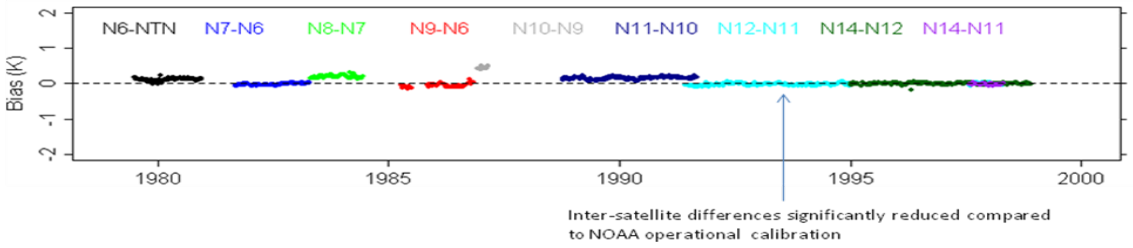

(b)

Figure 3-11 Global ocean-mean inter-satellite brightness temperature difference time series for MSU channel 2 onboard TIROS-N through NOAA-14 derived from (a) the NOAA operational calibrated radiances, and (b) radiances obtained from using SNO calibration coefficients.

3.4.2.2 The AMSU-A Calibration Coefficients

For AMSU-A observations, bias drifts and a combination of bias drifts and instrument temperature variability were observed in the pre-launch calibrated radiance time series for certain channels of NOAA-16 and MetOp-A. For these channels, constant offsets and nonlinear coefficients cannot remove their bias drifts. Therefore, time dependent offsets and nonlinear coefficients are introduced to account for the bias drifts (Zou and Wang, 2011). In specific, the following offset variation model is assumed for MetOp-A channel 7 and most NOAA-16 channels,

$$\delta R = \delta R_0 + \kappa(t - t_0) \qquad (3\text{-}3)$$

where δR_0 is a constant offset, λ is a constant rate of changes in the offset, *t* is time, and t_0 is a reference time which can be the satellite launch time or other reference time when the offset begins to change. Calibration results indicate that this offset model is sufficient to remove the bias drift in all channels except for NOAA-15 channel 6. For this channel, the nonlinear coefficient is also assumed to be time-dependent,

$$\mu = \mu_0 + \lambda(t - t_1) \qquad (3\text{-}4)$$

where μ_0 is a constant nonlinear coefficient, and κ is the rate of changes of the nonlinear coefficient, and t_1 is another reference time.

When solving for the calibration coefficients in Equations 3-3 and 3-4, δR_0 and μ_0 were obtained first from the SNO sequential procedure described earlier with λ and κ being assumed to be zero and NOAA-18 was used as the reference satellite. The resulting δR_0 and μ_0 were then fixed in Equations 3-3 and 3-4 in subsequent procedures where λ and κ values are determined. To obtain λ and κ, a series sensitivity experiments were conducted in which λ and κ were selected within a reasonable range and different set of level-1c radiances were computed corresponding to these different values. The final selection of λ and κ were made when the inter-satellite bias drifts of the global ocean means are minimal for all respective channels.

The resulting calibration coefficients for channels 4-14 onboard NOAA-15, -16, -17, -18 and MetOp-A are listed in Table 3-3. Aqua was recalibrated in the sense that only constant offsets were obtained since its raw counts are not easily acquired. Nevertheless, inter-satellite bias analysis as shown in Figure 3-12 indicated that no significant instrument temperature variability was found for all Aqua channels during the time period from its launch to present. Therefore, it is postulated that the non-linear calibration coefficients for Aqua AMSU-A may not need to be changed from operational values.

Table 3-3 SNO determined calibration coefficients for AMSU-A channels 4-14. For simplicity, all δR and μ were adjusted to the corresponding starting time shown in the equation (2001 for δR and 1998 for μ). These starting times were not necessarily set to be the exact launch time for a satellite. One can transfer them to the satellite launch time if needed by changing the values of δR_0 and μ_0. Calibration coefficients of AMSU-A surface channels 1-3 and 15 are not included. Units for δR_0, μ_0, κ, and λ are 10^{-5} (mW) (sr m^2 cm^{-1}) $^{-1}$, (sr m^2 cm^{-1}) $(mW)^{-1}$, (mW) (sr m^2 cm^{-1}) $^{-1}$ $(year)^{-1}$, and (sr m^2 cm^{-1}) $(mW)^{-1}(year)^{-1}$, respectively.

		δR_0	κ	μ_0	λ
Channel 4	NOAA-15	0	0	-0.269	0
	NOAA-16	0	0	-0.718	0
	NOAA-17	0.220	0	-0.886	0
	NOAA-18	0.276	0	0.929	0
	MetOp-A	0.324	0	0.442	0
	Aqua	-0.034	0	0	0
Channel 5	NOAA-15	0	0	0.3	0
	NOAA-16	-1.846	-7.248e-07	2.4	0
	NOAA-17	0.877	0	-1.007	0
	NOAA-18	0	0	1.468	0
	MetOp-A	0.467	0	0.262	0
	Aqua	0.023	0	0	0
Channel 6	NOAA-15	1.406	-0.614e-05	0	0.442
	NOAA-16	-2.903	-1.177e-06	4.3	0
	NOAA-17	5.065	0	-3.722	0
	NOAA-18	0	0	3	0
	MetOp-A	1.131	0	2.389	0
	Aqua	1.667	0	0	0
Channel 7	NOAA-15	0	0	0.3	0
	NOAA-16	-4.475	-1.570e-06	3.6	0
	NOAA-17	3.043	0	-2.347	0
	NOAA-18	1.319	0	0.479	0
	MetOp-A	2.152	-1.169e-06	0.396	0
	Aqua	-0.341	0	0	0
Channel 8	NOAA-15	0	0	0.667	0
	NOAA-16	-5.043	-1.768e-06	4.3	0
	NOAA-17	2.078	0	-1.099	0
	NOAA-18	0.440	0	0.964	0
	MetOp-A	1.633	0	0	0
	Aqua	-0.034	0	0	0
Channel 9	NOAA-15	0	0	0.077	0
	NOAA-16	-4.130	-3.936e-07	2.3	0
	NOAA-17	1.334	0	-0.809	0

	NOAA-18	-0.108	0	0.820	0
	MetOp-A	0.111	0	1.246	0
	Aqua	-1.403	0	0	0
Channel 10	NOAA-15	0	0	0.346	0
	NOAA-16	0.227	0	-0.200	0
	NOAA-17	0.711	0	-0.361	0
	NOAA-18	0.876	0	1.116	0
	MetOp-A	0.975	0	1.148	0
	Aqua	-0.189	0	0	0
Channel 11	NOAA-15	0.532	0	0.251	0
	NOAA-16	-0.788	2.910e-7	0.733	0
	NOAA-17	0.595	0	0.406	0
	NOAA-18	0	0	1.500	0
	MetOp-A	0.614	0	1.626	0
	Aqua	0	0	0	
Channel 12	NOAA-15	0	0	1.115	0
	NOAA-16	-0.300	-8.000e-7	1.600	0
	NOAA-17	1.752	0	0	0
	NOAA-18	3.390	0	0	0
	MetOp-A	3.662	0	0	0
	Aqua	1.754	0	0	0
Channel 13	NOAA-15	0	0	1.500	0
	NOAA-16	0.702	-8.045e-07	1.000	0
	NOAA-17	1.471	0	0	0
	NOAA-18	3.171	0	0	0
	MetOp-A	3.018	0	0	0
	Aqua	2.696	0	0	0
Channel 14	NOAA-15	0	0	0	0
	NOAA-16	-1.364	-0.154e-5	1.200	0
	NOAA-17	-0.514	0	0.712	0
	NOAA-18	0	0	0.600	0
	MetOp-A	-0.062	0	-0.435	0
	Aqua	0	0	0	0

The global ocean mean inter-satellite difference time series for channel 5, 6, 7, and 9 derived respectively from operational calibration and the calibration coefficients in Table 3-3, are shown in Figures 3-12 and 3-13. As seen, inter-satellite biases, sun heating induced instrument temperature variability, and bias drift are all found in Figure 3-12 in the operational calibration. These biases are all significantly reduced by the SNO calibration coefficients as shown in Figure 3-13. The biases and standard deviation of the inter-satellite difference time series in Figure 3-13 are typically on the

order of 0.05K and 0.03 K, respectively, compared to 0.5 K and 0.13 K in prelaunch calibration shown in Figure 3-12.

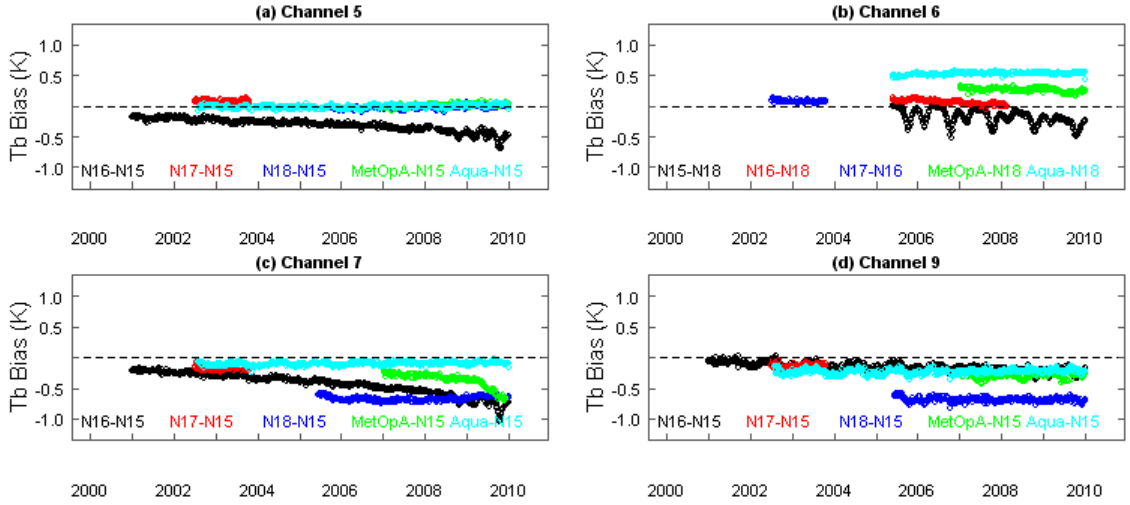

Figure 3-12 Global ocean-mean inter-satellite T_b difference time series for AMSU-A operational calibration for satellites NOAA-15, -16, -17, -18, MetOp-A, and Aqua for different channels. Differences are chosen against the reference satellites, thus the satellite pairs shown for channel 6 are different from other channels.

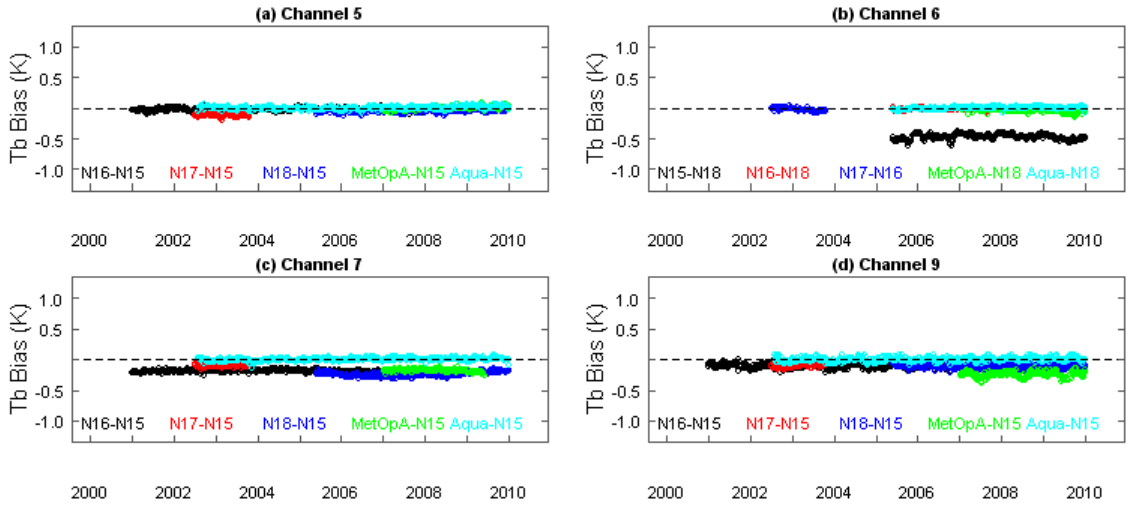

Figure 3-13 Same as Figure 3.12 except T_b is obtained using the SNO inter-calibration coefficients listed in Table 3-3. Note the large differences between NOAA-18 and NOAA-15 for channel 6 is caused by post-launch frequency shift in NOAA-15 channel 6. The correct frequency for NOAA-15 channel 6 has been obtained in Zou and Wang (2011), which is 36.25 MHz higher than pre-launch specification or measurements.

3.4.3 Numerical Strategy

The computation of SNO recalibrated radiances is straightforward using Equation 3-1 given the calibration coefficients and raw counts data of the Earth views, target

views, and other necessary parameters from the MSU/AMSU level-1b files. Processing the large amount of AMSU level-1b files and saving the resulting level-1c files require tens of Terabytes of disk space storage. Frequent update of the disk storage and workstations for processing the dataset needs to be planned.

3.4.4 Calculations

The algorithm steps for generating the radiances are as follows:

1) Read ancillary datasets including calibration coefficients

2) Processing each MSU/AMSU level 1b orbit file

   - Read level 1b header
   - Process each scan line
     - Parse scan line
     - Calibrate scan line using Equation 3-1 for each footprint
     - Run precipitation detection program to identify if the footprint observation is precipitation contaminated
     - Run quality control program to ensure the calibrated radiance is valid
   - Generate Level-1c radiance file
   - Output the Level-1c file using NetCDF format

3) Repeat step 2) for another L1b orbit file

4) Stop after all level 1b files are processed

3.4.5 Algorithm Output

The MSU/AMSU-A atmospheric temperature channel radiances recalibrated using the SNO method are the major outputs from the algorithm. Quality flags are produced to indicate product quality, invalid or missing data. The algorithm also outputs NOAA pre-launch calibrated and linear calibrated radiances.

Table 3-4 Parameters in the supplied sample output data.

Parameters	Explanation
SNO recalibrated radiances	Recalibrated atmospheric temperature channel

	radiances MSU: channels 2-4 AMSU-A channels 4-14
NOAA pre-launched calibrated radiances	NOAA pre-launched calibrated radiances MSU: channels 1-4 AMSU-A channels 1-15
Limb effect corrected SNO recalibrated radiances	Recalibrated and limb effected corrected atmospheric temperature channel radiances MSU: channels 2-4 AMSU-A channels 4-14
Limb effect corrected NOAA pre-launched calibrated radiances	NOAA pre-launched calibrated and limb effect corrected radiances MSU: channels 1-4 AMSU-A channels 1-15
Quality control	Scan line and pixel/channel level quality control information based on Level 1b quality control and level 1c precipitation screening and limb correction algorithms.

4. Validating Datasets and Algorithm Accuracy

4.1 Validating Datasets

Determination of accuracy and precision of the SNO inter-calibration algorithm and its resulting FCDR are segmented into two parts: relative error estimates between satellite pairs and absolute error estimation with respect to an absolute truth. The purpose of the SNO method is to improve inter-satellite calibration; evaluation of the relative errors between satellite pairs is thus the primary goal in the algorithm validation process. However, absolute error estimate should also be carried out whenever possible since improving absolute accuracy is the ultimate goal of any calibration process. Ideally, absolute error estimate should be made against a SI-traceable standard of the microwave observations. However, such a standard does not exist at the time of this writing; therefore, various vicarious validation data sources are examined to determine their validity for validating the absolute accuracy of the SNO inter-calibration algorithm. Such vicarious data sets are also rare due to the strict criteria required for a dataset to be of climate quality for validating other data sets: high precision and accuracy traceable to SI standards, long-term availability and stability, and global coverage with homogeneity. Since accuracy estimates for a calibration algorithm actually depend on the accuracy of the vicarious datasets themselves, cautious views of the estimating results are recommended. After reviewing available long-term temperature datasets in the climate science community, it is concluded that only the multi-year (2001-present) temperature retrievals from the Global Positioning System (GPS) Radio Occultation (RO) and reanalysis datasets have the potentials to

serve as vicarious datasets to validate the SNO calibrated MSU/AMSU radiances. Estimates of the relative accuracy of the SNO calibration algorithm are made against those from pre-launch calibrations. The characteristics of these datasets and their comparison results with the SNO calibrated MSU/AMSU observations are described as follows.

4.1.1 Pre-launch calibrated MSU/AMSU radiances

Advantages of the SNO calibration algorithm are established by comparing inter-satellite biases against those from the pre-launch calibration. Pre-launch calibration is conducted independently for each instrument where calibration offsets are assumed to be zero and nonlinear calibration coefficients are obtained from laboratory test datasets (e.g., Mo, 2006). Time-varying inter-satellite biases exist for these instrument observations after launch. These data are available in the operational MSU/AMSU L1b files and they have been widely used in NWP data assimilations to improve NWP weather forecasting. The inter-satellite bias characteristics of the pre-launch calibrated datasets are used as reference for the SNO calibration to compare with and for understanding the improvement of the latter algorithm compared to the former algorithm.

4.1.2 GPSRO data

The GPSRO data are provided by receivers onboard low Earth orbiting (LEO) satellites. As an LEO satellite sets or rises behind the Earth's limb relative to the GPS transmitter satellite, the onboard GPS receiver takes measurements of the phase and amplitude of the GPS signals. These phase measurements, together with the precise knowledge of the positions and velocities of the GPS and LEO satellites, can be collectively used to derive accurate information (< 0.5 Kelvin temperature accuracy between ~5-25 km) on the thermodynamic state of the atmosphere. GPS RO data are minimally affected by aerosols, clouds, or precipitation and are not expected to have instrument drift and satellite-to-satellite instrument bias. Current evidence shows that temperature profiles acquired with GPS RO are absolutely stable at a level of <0.05 Kelvin between ~10-25 km, where the water vapor effects are small. In the middle and lower troposphere, refractivity datasets can be used instead of temperature, thus combining the temperature and moisture information.

In contrast to the microwave sounders, the raw GPS RO measurement is not based on a physical device that deteriorates with time — their performance is directly traceable to an absolute SI standard: International Atomic Time. Consequently, there is no need for calibration. This makes this limb-sounding technique extremely useful for calibration of other nadir sensors. Even if the span period of available RO measurements is not long enough (2001-present) to build GPS RO time series for climate applications yet, it can still be used to validate other observations such as MSU/AMSU stratospheric channels.

4.1.3 Reanalysis datasets

Reanalysis data were generated from long-term runs of fixed climate modeling systems with combinations of a comprehensive set of physical parameterizations and assimilation of routine observations from various sources such as satellites, ships, buoys, aircraft, and the radiosonde network, etc. The data assimilation process allows reanalysis to have a climate state favorable to certain input data, depending on human knowledge of bias nature of various input data as well as an appropriate bias correction scheme for the input data. Current generation of reanalysis systems employs a satellite bias correction scheme in their data assimilation sub-systems. Satellite bias correction is a process to correct errors in satellite observations, including MSU/AMSU radiance data, before they are assimilated in modeling reanalysis systems. This correction is implemented based on the assumption that satellite data are less accurate compared to in situ observations such as those from radiosondes and aircrafts, which are not subject to bias correction before being assimilated into reanalysis systems. As such, when there is a disagreement between the satellite and radiosonde and aircraft observations, reanalysis data assimilation tends to generate a climate reanalysis favorable to the radiosonde and aircraft observations. Since in situ observations have biases relative to the absolute truth and are also subject to in-homogeneity in both time and space, the reanalysis data in principle cannot be treated as vicarious datasets for evaluating the absolute accuracy of the recalibrated MSU/AMSU FCDRs. Reanalysis developed by different operational centers are also different due to differences in their production processes which include climate model differences as well as different choices in input datasets and data assimilation schemes. These differences also cause difficulties in selecting appropriate reanalysis data for validating other climate datasets. Therefore, using reanalysis data to investigate the climate change or validate other dataset still comes a long way to go.

Despite these deficiencies, however, satellite bias correction techniques and their analysis are a unique tool that can provide independent assessment of the recalibration accuracies of the SNO calibration algorithm. In particular, the bias correction patterns for individual satellite can be used to examine how well instrument calibration was conducted when compared to a reference climate favorable to in situ observations. New generation of reanalyses cover the entire satellite observation period, allowing algorithm performance evaluations for the entire satellite observation period. An analysis example will be provided in the following sections to demonstrate this feature.

4.2 Algorithm Accuracy Analysis

4.2.1 Reproducibility

Based on characteristics of the validating datasets, different statistical methods are developed to determine the accuracy of the SNO calibration algorithm. These include

a) In comparisons with pre-launch calibration, four statistical parameters are used to characterize the accuracy of the SNO calibration. The details are described in the next section.

b) For GPSRO datasets, matched pixel observations of the MSU/AMSU and GPSRO data are first collected. Bias statistics of these matchups can characterize the accuracy and precision of the SNO recalibrated MSU/AMSU radiances against GPSRO observations.

c) For reanalysis datasets, bias correction analysis of the SNO calibrated radiance data is conducted. These bias correction analyses provide a fundamental understanding on the performance of the SNO calibration algorithm in terms of how inter-satellite biases are removed when compared to a common reference dataset.

4.2.2 Precision and Accuracy

4.2.2.1 Relative Accuracy

Four parameters/indexes have been developed to evaluate the relative accuracy of the SNO calibration algorithm between satellite pairs. These different parameters/indexes characterize different aspects in the instrument calibration errors. Advantages of the SNO calibration algorithm are established by comparing values of these parameters against those from the pre-launch calibration.

i) Mean inter-satellite biases between SNO mathchups—give an estimate of the relative offsets between two satellites. The relative offsets arise from many different sources of calibration errors between satellite pairs: different offsets of the blackbody calibration targets, slight differences in antenna pattern corrections, differences in satellite height, etc. In pre-launch calibrated radiances, these biases are generally non-zero and are on the order of 0.3 to 1 K. An example has been shown in Figure 3-8a for the SNO matchups of MSU channel 2 between NOAA-10 and NOAA-11, where pre-launch calibrated radiances for the nadir pixels have a mean bias of 0.3 K. By definition, the SNO regression algorithm completely removes this bias, at least for the near nadir observations. As shown in Figure 3-8b, this bias is reduced to zero after the SNO calibration.

ii) Scene temperature dependency in the inter-satellite biases — give an estimate of the non-uniformity in inter-satellite biases. This type of biases occurs when calibration nonlinearity is inaccurate or when channel frequencies of two instruments are different. Bias structure in the scatter plot must be analyzed in order to determine the exact root-causes of the biases. In general, scene temperature dependent biases due to inaccurate calibration nonlinearity are characterized by a simple linear slope in the SNO scatter plot between two satellites (Figure 3-8), while those related to channel frequency differences have more complicated structures in the inter-satellite bias scatter plots. Fortunately, the first type of biases occurs more often than the second one. In addition, scene temperature dependency in biases causes the biases to depend on the latitudinal

zones and seasons. The seasonal cycles in the SNO time series are thus defined as an associated parameter in characterizing the calibration accuracy in reducing scene temperature dependency in biases. The SNO inter-calibration algorithm finds optimum nonlinear calibration coefficients which significantly reduce scene temperature dependent biases (Figure 3-8). As seen in Figures 3-8a and 3-8b, the SNO inter-calibration reduced the slope in the scatter plot by 3 times. Figure 4-1 shows another example of this type of biases between MetOp-A and NOAA-18 where seasonal cycles in the SNO time series are associated with slope in the SNO scatter plot between the two satellites. After SNO inter-calibration, the slope and the seasonal cycles in the SNO time series are both significantly removed.

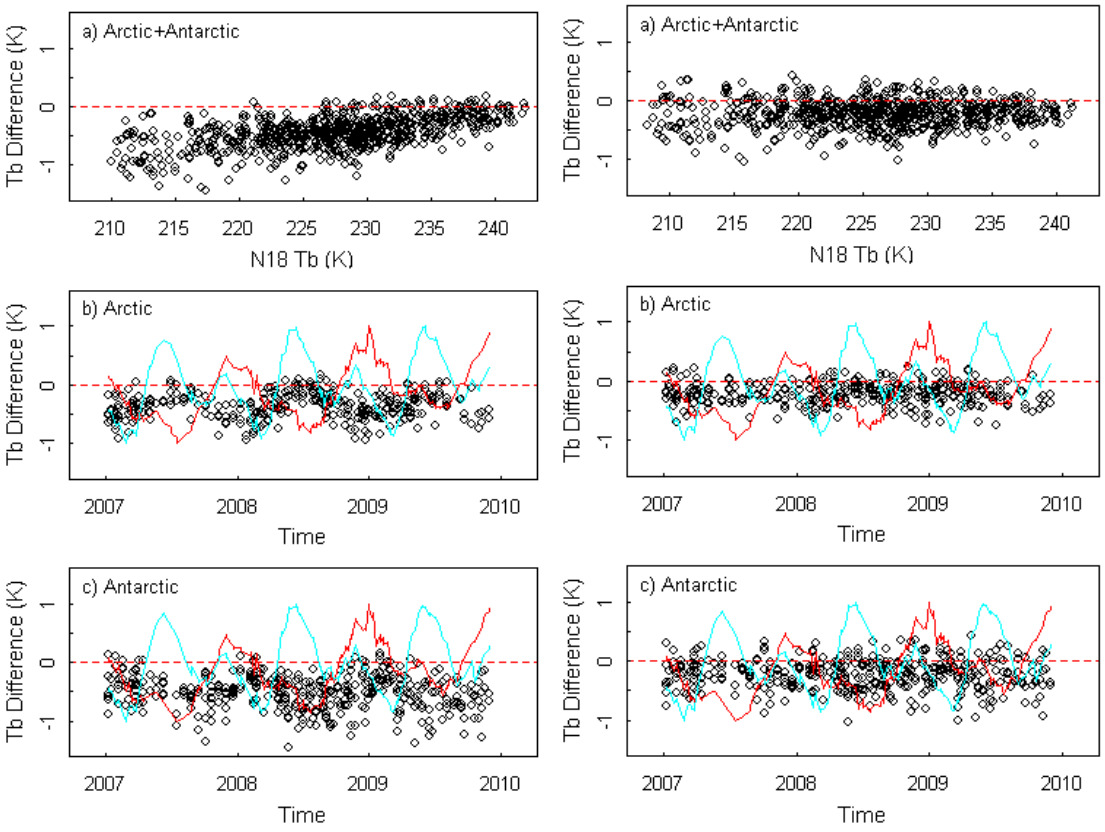

Figure 4-1 LEFT: a) SNO scatter plot for $T_b(N18)$ versus $\Delta T_b = T_b(MetOp-A) - T_b(N18)$; b) SNO time series for T_b (MetOp-A) - T_b (N18) over the Arctic; c) Same as b) except over the Antarctic. The T_b data in these plots were derived from unrealistic non-linear calibration coefficients assigned to both NOAA-18 and MetOp-A. The red and blue curves in b) and c) are the warm target temperature time series for MetOp-A and NOAA-18, respectively. The out-of-phase seasonality in the Arctic and Antarctic SNO time series cannot be explained by the warm target temperatures of either MetOp-A or NOAA-18. RIGHT: Same as LEFT except they are derived from SNO calibration coefficients.

Scene temperature dependent biases caused by channel frequency shift and their associated seasonal cycles in the Arctic and Antarctic SNO time series have been shown in Figure 4-2 for pre-launch calibrated NOAA-15 and NOAA-18 channel 6 observations. After adjustment using the realistic channel frequency value obtained from CRTM simulations, the scene temperature dependent biases in the SNO scatter plots between NOAA-15 and NOAA-18 and their SNO seasonal cycles are both removed (Figure 4-3).

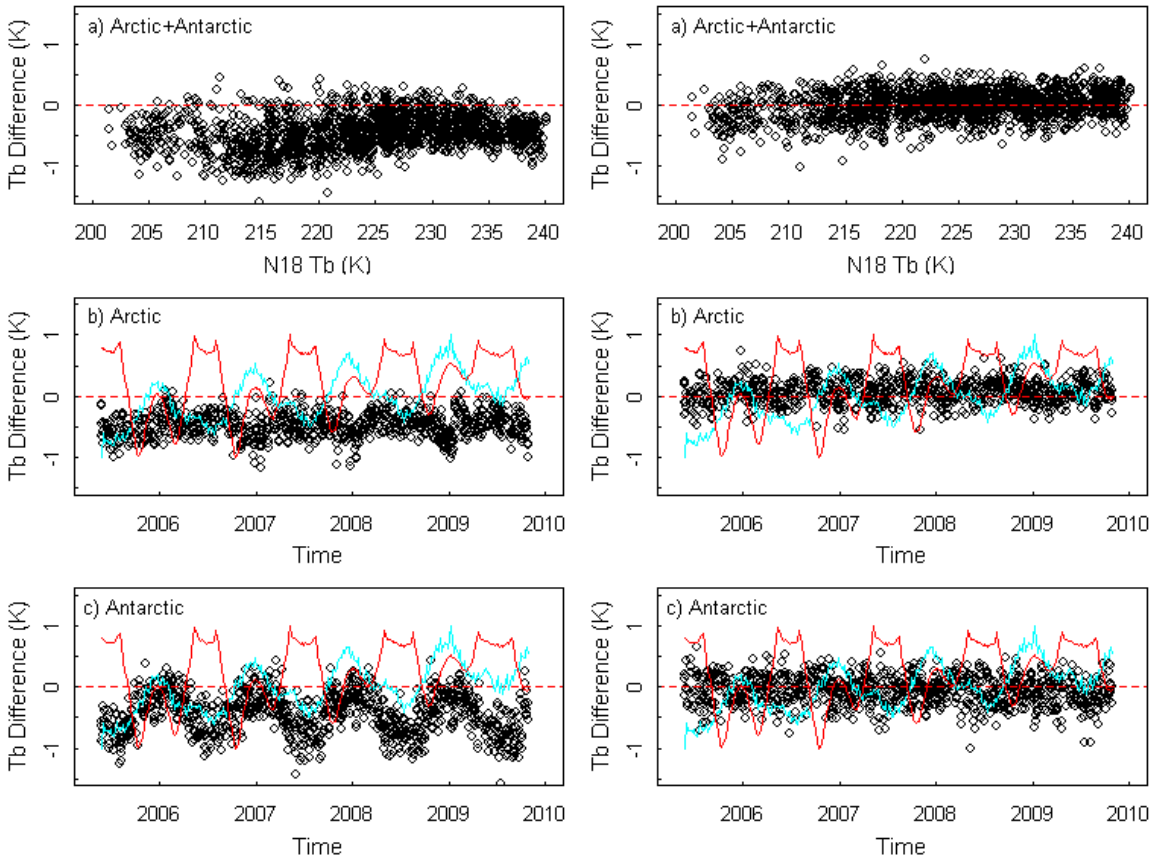

Figure 4-2 (LEFT Panels) a) SNO scatter plot for $T_b(N18)$ versus $\Delta T_b = T_b(N15) - T_b(N18)$; b) SNO time series over the Arctic for $\Delta T_b = T_b(N15) - T_b(N18)$; c) Same as b) except over the Antarctic. The T_b data in these plots were derived using the calibration coefficients in Table 3-3 where calibration non-linearity related scene temperature-dependent biases have already been minimized in the SNO calibration procedure. In addition, NOAA-15 offset has been adjusted to account for its frequency shift, so its T_b values are lower than operational calibrated values by a constant. The red and blue curves in b) and c) represent respectively the warm target temperatures of NOAA-15 and NOAA-18.

Figure 4-3 (RIGHT Panels) Same as Figure 4-2 except for the adjusted SNO time series between NOAA-15 and NOAA-18 in which the CRTM simulated differences due to the NOAA-15 frequency shift was subtracted from the observed NOAA-15 T_b.

iii) Latitudinal dependency in biases: Since the temperature range of the SNO mathcups is slightly smaller than the global temperature range, removing biases and the seasonal cycles in the SNO matchups does not guarantee that biases are removed over the globe. It is desirable to examine scene-temperature-dependent biases in global datasets after the SNO calibration. Latitudinal dependency in inter-satellite biases provides additional information on the calibration accuracies. Figure 4-4 shows the spatial pattern of the time-averaged T_b differences for NOAA-11 minus NOAA-10, NOAA-12 minus NOAA-11, and NOAA-14 minus NOAA-12 during their overlapping observations. These figures include MSU channel 2 (T_2), channel 3 (T_3), and channel 4 (T_4) products. The figure shows that the biases are within ±0.1 K over the ocean and most of the land areas for the NOAA-14 minus NOAA-12 fields of T_3 and T_4 (Figure 4-4f). Similar bias level is also found for the differences between NOAA-12 and NOAA-11 and NOAA-14 minus NOAA-12 of T_2 over the oceans (Figure 4-4b,c). This shows the SNO calibration works well over the globe for these overlaps. The NOAA-11 minus NOAA-10 of T_3 (Figure 4-4d) and the NOAA-12 minus NOAA-11 of T_4 (Figure 4-4h) show medium biases (±0.2 K) over the tropics. However, relatively larger differences (about 0.3 K) near the peaks of the Andes and Himalaya mountains are found for all overlaps for T_3 (Figure 4-4d–f). These larger differences occur because the surface elevation at these geographic locations is so high that the diurnal drift effect has a larger contribution to the channel 3 observations. For land areas with lower elevations, the diurnal drift effect is negligible for channels 3 and 4 as the inter-satellite biases over these areas are the same as over the oceans. In any situation, however, the diurnal drift effect for channel 2 is important over land because bias differences between land and oceans are more apparent (±1K over land but 0.2 K over oceans, Figure 4-2a–c). The NOAA-11 minus NOAA-10 of T_2 and T_4 (Figure 4-4a,g) and the NOAA-12 minus NOAA-11 for T_3 (Figure 4-3e) show larger latitudinal dependency, with smaller magnitude over the polar region and larger values over the tropics. This latitudinal dependency in biases suggests that a single calibration coefficient for the nonlinear term cannot completely remove the scene temperature dependency in biases. It is very likely that more terms and coefficients in the calibration equation are required for more accurate calibration when the quadratic approximation does not perform well.

iv) Inter-satellite biases of the global ocean mean time series—Although many calibration features can be characterized by the SNO matchups, global-ocean mean difference time series provide additional information on the bias characteristics of the calibrated radiances. This is because (a) global-ocean mean data include global temperature range which is larger than those from the SNO matchups which occur only over the polar region; (b) For many channels, global-ocean means do not have significant diurnal drift errors so they can still be used to characterize the instrument calibration errors; and (c) sample noise due to time and space differences in the SNO matchups is mostly cancelled out in the global ocean averaging processes so its difference time series can be used to characterize some fine features such as the instrument temperature variability and long-term drift in the satellite radiance observations. By comparing the MSU global-ocean mean difference time series between satellite pairs before (Figure 3-11a) and after (Figure 3-11b) the SNO calibration, the advantage of the SNO calibration algorithm are seen from the following bias statistics: a) the inter-satellite biases in Figure 3-11b are about 0.1 K for the well-

calibrated satellites such as NOAA-10 through NOAA-14, comparing to 0.5 K - 1 K in the pre-launch calibrated time series (for channel 3, inter-satellite biases as large as 2 K were observed in the pre-launch calibrated time series); b) warm target temperature variability are mostly removed in the SNO calibration, resulting in the standard deviation of the global-ocean mean difference time series of only 0.03 K, compared to 0.12 K in the pre-launch calibrated time series (Figure 3-11a); c) there is no obvious bias drift in the SNO calibrated difference time series for all satellite pairs, while the bias drift in the pre-launch calibration is quite obvious, for example, between NOAA-12 and NOAA-14.

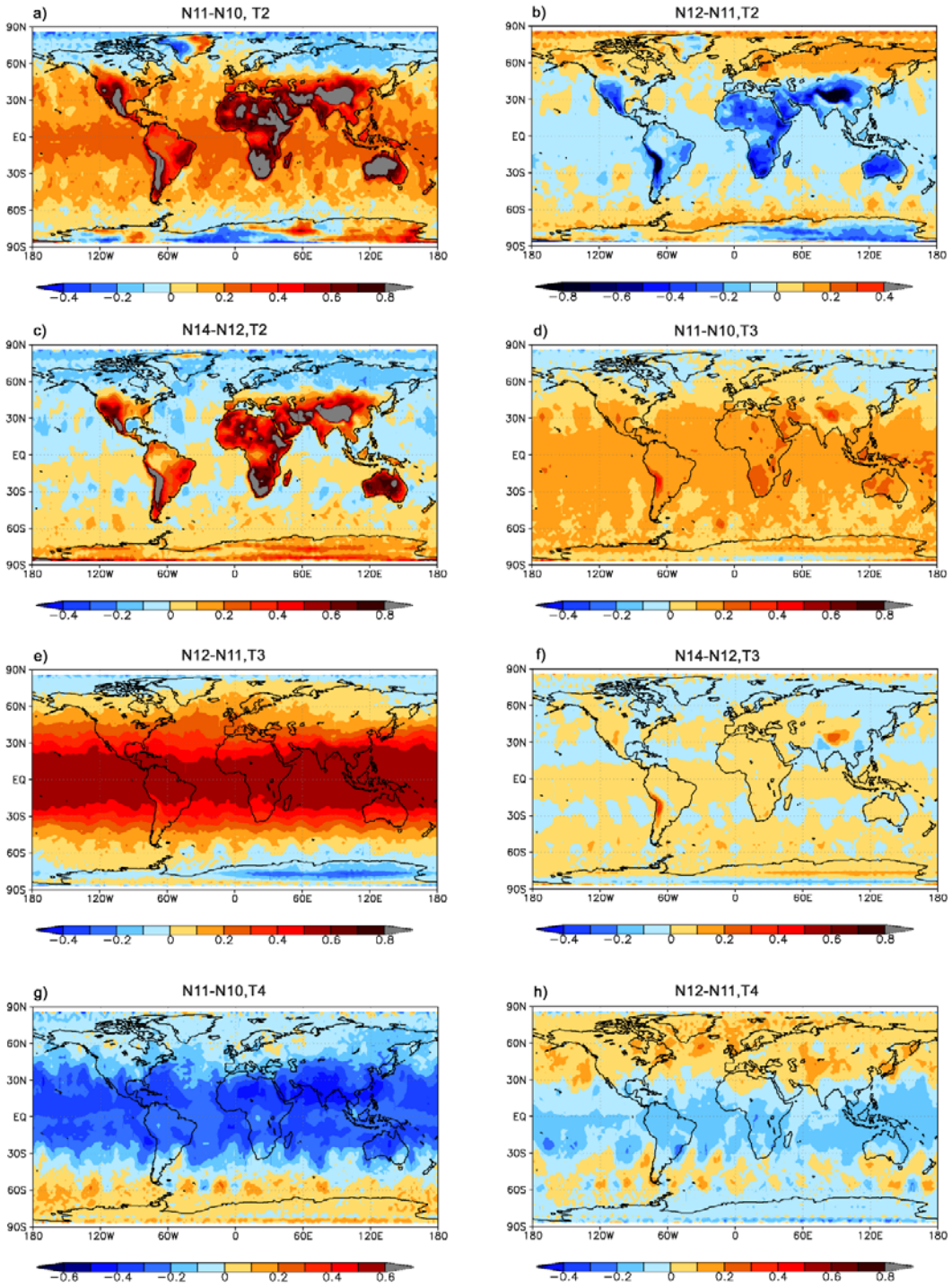

Figure 4-4 Intersatellite bias patterns for different satellite overlaps for different channels after the SNO calibration. A total of 7 limb-corrected footprints per scanline are used in the pentad dataset. Units are in K.

4.2.2.2 Comparisons against GPSRO for Absolute Accuracy Estimates

Figures 4-5 and 4-6 compares the COSMIC retrievals with the AMSU-A channel 9 T_b derived from the SNO calibration and the operational calibration for a randomly selected time period, July 2007. The comparisons are divided into three regions: Arctic (60°N-90°N, red dots), Antarctic (60°S-90°S, blue dots), and the rest of the Earth (60°N-60°S, green dots). Near nadir (the 15th footprint) and near limb (the 30th footprints) comparisons are provided separately. Table 4-1 further summarizes the bias statistics in the comparison.

The mean biases of the SNO calibrated radiances are only of 0.01 K to 0.04 K for both the near nadir and near limb footprints, compared to a bias of about 0.30 K in the pre-launch operational calibrated data. This shows an obvious improvement from the SNO calibration. Regional biases such as those over the Antarctic are much larger for both the SNO and operational calibrations (0.3 K for SNO and 0.8 K for the operational calibration) than those in the 60°N-60°S region. This suggests that either the COSMIC has a larger retrieval error (the GPSRO temperature was retrieved from the bending angle) or the AMSU data are downgraded over the polar region in both the SNO and pre-launch calibrations. The SNO uses two single parameters (nonlinear coefficient and offset) and two targets to calibrate the raw counts data. It is not likely that this calibration is downgraded over the polar region. Therefore, the problem is most likely related to deficiencies in the COSMIC retrievals. For instance, the polar stratospheric clouds may affect the accuracy of the COSMIC retrievals. This problem is being investigated at the time of this writing. This indicates that the comparison is not only helpful in estimating the absolute accuracy of the SNO calibrated radiances, but in turn, it is also helpful in identifying the potential problems in the validation dataset itself.

In addition, the slope of the SNO calibration is closer to 1 in both the near nadir comparison and near limb comparisons, suggesting less scene temperature dependency in biases in the SNO calibrated radiances. These statistics indicate that the SNO calibrated data are of higher accuracy and quality compared to the prelaunch calibration.

Table 4-1 Bias statistics in comparisons between COSMIC retrievals and the NOAA-15 AMSU-A channel 9 T_b for July 2007. The comparisons include operational (OPE) and the SNO calibrated radiances (Table courtesy of Dr. Wenying He at Institute of Atmospheric Physics, China).

200707 N=957	**60°S-60°N**	**60°N-90°N**	**60°S-90°S**	**Global**
OPE-COSMIC	-0.25	-0.06	-0.82	−0.30
SNO-COSMIC	-0.01	0.07	-0.31	−0.04

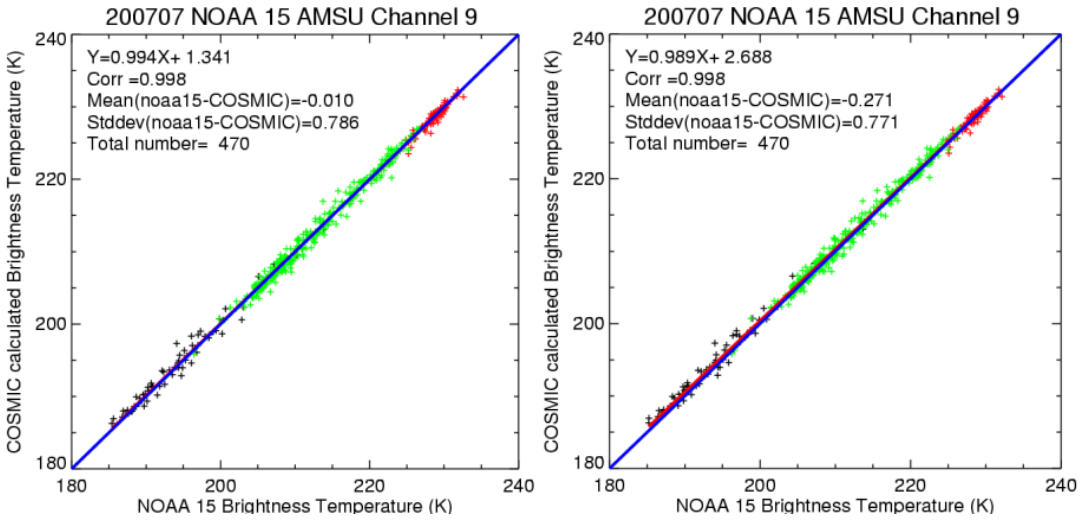

(a) (b)

Figure 4-5 Scatter plot between the AMSU-A channel 9 brightness temperature at the 15th footprint onboard NOAA-15 and the collocated COSMIC retrievals during July 2007. The red dots represent the Arctic (60°N-90°N) data, the blue dots the Antarctic (60°S-90°S) data, and the green dots for the rest of the Earth (60°N-60°S). (a) SNO calibrated radiances versus COSMIC; (b) Operational calibrated radiances versus COSMIC (Plots courtesy of Dr. Wenying Wang, Institutes of Atmospheric physics, China)

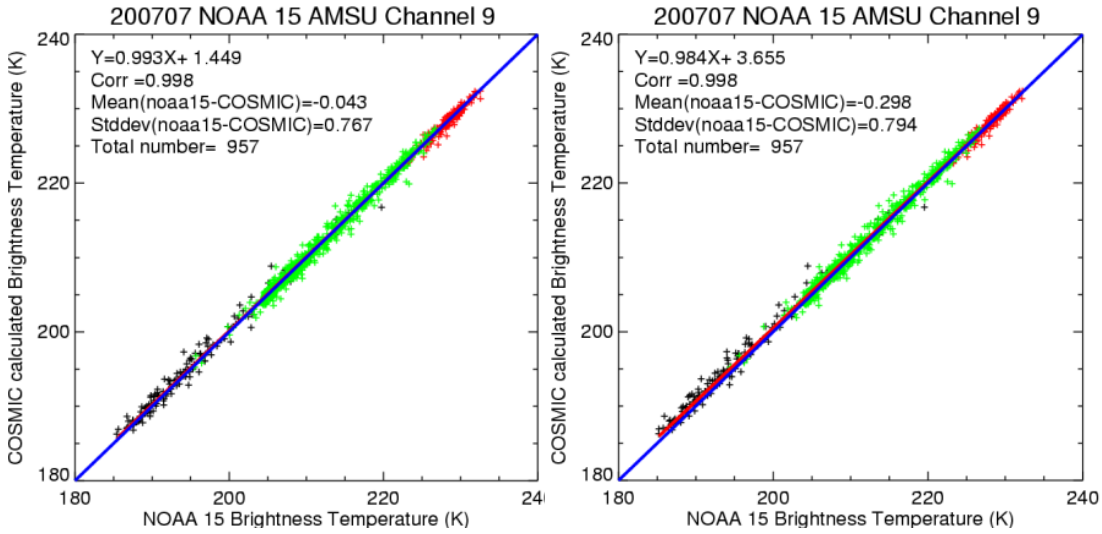

(a) (b)

Figure 4-6 Same as Figure 4-5 except for the 30th footprint.

4.2.2.3 Bias Corrections in Reanalysis

The SNO calibrated FCDR is expected to have good impact on the reanalysis bias correction process since the instrument calibration errors have been minimized. As an effort to test the performance of the inter-satellite calibration for climate reanalysis improvement, 20-years (1987-2006) of SNO calibrated MSU level-1c radiances for channels 2, 3 and 4 onboard NOAA-10 through NOAA-14 were assimilated into the new generation of NCEP Climate Forecast System Reanalysis (CFSR) (Saha et al., 2010) and NASA Modern Era Retrospective-analysis for Research and Applications (MERRA) reanalysis (Rienecker, et. al. 2011). Since the CFSR and MERRA reanalysis cover the entire period of MSU observations from 1978 to 2006, they actually assimilated two different MSU level-1c data: the NOAA operational calibrated for TIROS-N through NOAA-9 and the post-launch SNO calibrated for NOAA-10 through NOAA-14. The fact that radiances from these different calibration procedures were assimilated into a same system serves as an ideal experiment for evaluating the impact and performance of the SNO inter-satellite calibration effort. Figure 4-7 shows the total bias correction patterns of MSU channel 2 in CFSR for the eight satellites from NOAA-6 through NOAA-14. The total bias correction is a global mean difference between the satellite observations being assimilated in the reanalysis and a background forecast field used to evaluate the observation biases. In many situations, the total bias correction is nearly the same as the difference between the observations and the final reanalysis field (O-M). Therefore, the total bias correction is an indicator of how well climate reanalysis agrees with the observations. The total bias correction for different satellites also measures the difference or agreement between different satellites, since double differencing of the bias corrections between two satellites leads to the same results as the inter-satellite bias analysis shown in Figure 3-11.

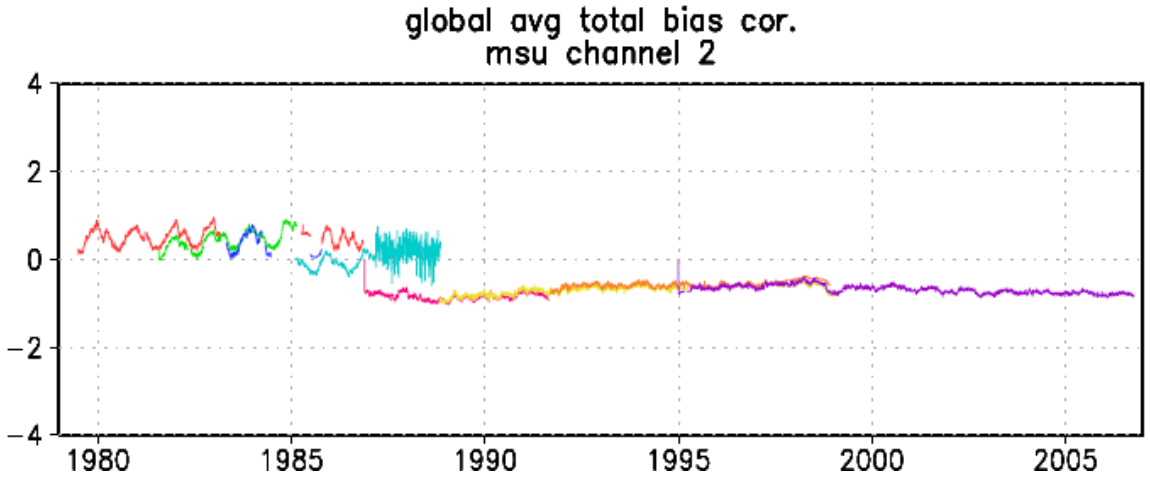

Figure 4-7 Four times daily averaged, global-mean total bias correction (Kevin) for MSU channel 2 onboard satellites from NOAA-6 through NOAA-14. The time series from 1979 to 1988 in 4 different colors (with larger seasonal variability) are for NOAA-6 through NOAA-9, and the smoother time series from 1987 to 2007 in other 4 different colors are for NOAA-10 through NOAA-14 (Plot from (Saha et al., 2010)).

In Figure 4-7, the bias corrections for NOAA-6 through NOAA-9 exhibit obvious seasonal and inter-annual variability. This variability is related to the sun heating induced instrument temperature variations. In addition, the bias correction values for NOAA-6 through NOAA-9 are different for different satellites, indicating larger relative offsets between these satellites. This occurs because each individual satellite was calibrated independently in pre-launch calibration. In contrast, no instrument temperature variability is observed in bias corrections of the SNO calibrated MSU observations for NOAA-10 through NOAA-14. Moreover, the bias correction values for NOAA-10 through NOAA-14 are nearly the same, resulting in much consistent bias correction patterns for these satellites. With a double differencing of the bias corrections for the SNO calibrated satellites, one can see that the bias corrections are consistent with Figure 3-11 where inter-satellite biases are quite small for NOAA-10 through NOAA-14. In summary, bias correction pattern analyses indicate that the inter-calibrated MSU data have reached their performance expectation in reanalysis data assimilation.

One remaining problem is that there exist relative biases between the reanalysis climate and recalibrated satellite observations. Part of these errors may come from the climate reanalysis since it is not the truth. The other reason is that the absolute value of the inter-calibrated MSU/AMSU brightness temperature has not been adjusted to an absolute truth, although inter-satellite biases have been removed. As described earlier, the calibration offset of the reference satellite was arbitrarily assumed to be zero. This assumption does not affect the variability and trend analysis of the subsequent products developed from the FCDR. However, it influences the relative biases between the reanalysis and FCDR. This offset needs to be determined in FCDR validation processes against certain reference observations, ideally SI-traceable standards. Plans for such a validation are being developed at NOAA/NESDIS as part of the effort of MSU/AMSU FCDR development.

4.2.3 Error Budget

Table 4-2 summarizes the errors in the SNO calibrated radiance FCDR.

Table 4-2 Error Budget in the SNO calibrated radiances.

Error Type	Error Range	Comments
Calibration Uncertainty	0.5 - 1 K	This is total absolute uncertainty in instrument calibration.
Stability of Calibration Uncertainty	0.05-0.1 K/Decade	This stability is a measurement of bias drift relative to a benchmark climate observations that is considered as no error drift

Relative stability of Calibration Uncertainty	0.02 K/Decade	Relative bias drift between satellite pairs are small after bias drifts are minimized in the SNO inter-calibration
Scene temperature dependent biases due to inaccurate calibration non-linearity	0.02 K/K	This is the worst estimate for instrument channels that are not well represented by quadratic calibration equation. For most well calibrated satellite channels, this value can be as small as zero.
Noise equivalent temperature	0.2-0.3 K	This is a post-launch performance value for most channels. For AMSU channel 14, this value is about 0.6 K.
Global mean inter-satellite biases	0.1-0.2 K	
Standard deviation of global mean inter-satellite differences	0.03 K	This is the value for most tropospheric channels. For stratospheric channels, this value can reach 0.07-0.08 K for certain satellite pairs

5. Practical Considerations

5.1 Numerical Computation Considerations

Swath scene temperature fields dominate the storage requirements in the MSU/AMSU FCDRs. Compared to MSU (4 channels and 11 spots per scan line), AMSU-A has 15 channels and 30 footprints per scan line. Moreover, AMSU-A features a finer spatial resolution (45 km at nadir) than MSU (110 km at nadir). Under the same software and data design, the required disk space of AMSU-A is more than 20 times larger than that of MSU; the processing time for AMSU-A would also be more than 20 times longer. Therefore, different strategies were used to address disk space and processing time issues in MSU and AMSU-A.

(1) **Data type of temperature fields:** MSU data volume is relatively small (~ 70 GB), hence all temperature fields are stored in floating point format (4 bytes), which is convenient for data users. For AMSU-A, brightness temperature field supports two formats: scaled integer (2 bytes) and floating point. Scaled integer format can reduce storage space to half of that required by floating point format. However data users need to convert the scaled integers to floating point numbers and the precision of temperatures is thus reduced (0.01 K, but still sufficient for climate trend studies).

(2) **Parallelization**: To speed up the AMSU-A processing, multithreading technique was employed in its FCDR software code. This technique allows a computer program to run faster on a computer system that has multiple CPUs, CPU with multiple cores, or across a cluster of machines. The parallelization was implemented at level-1b file level, i.e., multiple AMSU-A level-1b files can be processed simultaneously to generate level-1c files.

5.2 Programming and Procedural Considerations

MSU and MSU/A FCDR software packages do not implement any numerical model.

5.3 Quality Assessment and Diagnostics

Percentage of missing/bad pixels in each level 1c file is monitored as an indicator of product quality. Missing or bad pixels are identified using the following diagnostics procedures:

(1) **Invalid level 1b file** is identified using NOAA Polar Orbitor Data User's Guide (for MSU) and KLM User's Guide (for AMSU-A) format specifications. If a header record error is identified, all scan lines will be flagged as bad.

(2) **Invalid time in level 1b files**. Two types of invalid time may exist in MSU and AMSU-A level 1b files: (1) invalid starting/ending time in header record; (2) invalid time in data record. A level 1b file with invalid starting and/or ending times will be flagged as bad file. A scan line with an invalid time will be flagged as bad scan line.

(3) **Invalid or missing geolocation**. Any pixel with an invalid or missing geolocation will be flagged as an invalid pixel.

(4) **Invalid or missing raw counts or warm target temperatures**. No calibration will be conducted in this case. Corresponding scene temperatures will be set to missing value (-9999) and its pixel level quality control flag will be set to 1.

(5) **Invalid scene temperatures**. All temperature values in MSU channels 2-4 and AMSU-A channels 4-14 will be compared to the Product Measurement Range given in Tables 2-1 and 2-2. Any pixel at any channel with invalid temperature will be replaced by missing value. Corresponding pixel level quality control flag will also be set to 1.

(6) **Precipitation screening**. Precipitation screenings for MSU channel 2 and AMSU-A channel 5 are implemented to screen out suspicious brightness temperatures associated with precipitation. Precipitation pixels will be replaced by missing values, and corresponding pixel level quality control flag will be set to 1.

Overall product quality is also assessed by analyzing randomly selected daily mean images of the brightness temperatures of individual satellite. Suspicious temperatures over certain locations may suggest bad data have passed through the processing codes.

5.4 Exception Handling

Exceptions that were considered in the MSU and AMSU-A FCDR processing codes include:

(1) **Class Not Found Exception** will be reported and the system stops running when the AMSU-A processing code tries to load in a class but no definition for the class could be found due to misplacement of external libraries.

(2) **Out of Memory Exception** will be identified when the system cannot allocate a block a memory because it is out of memory. If this exception occurs, the system will report the exception and exit running.

(3) **File Not Found Exception** will be reported and the system exits running when a calibration coefficients file, a limb correction coefficient file, or the land type file does not exist. It will also be identified if the file does exist but for some reason is inaccessible.

(4) **EOF Exception** will be reported when an end of file has been reached unexpectedly during file reading operations. If this exception occurs during reading a level 1b file, the system will stop processing the file, report the exception, and continue to process next file. If this exception occurs during reading a calibration coefficients file, a limb correction coefficient file, or the land type file, the system will exit running.

(5) **IO Exception** will be reported and the system stops running when a failed I/O operation, other than 3 and 4, occurs.

5.5 Processing Environment and Resources

Table 5-1 lists the environment and resource required by the MSU and AMSU-A FCDR processing codes:

Table 5-1 MSU and AMSU-A processing and environment and resource requirements.

	MSU	**AMSU-A**
Computer hardware	Minimum Configuration: Processor: 2.0 GHz Memory: 100 MB Disk space: 75 GB	Minimum Configuration: Processor: 2.0 GHz Memory: 200 MB Disk space: 900 GB A system with multiple CPUs is

		preferred.
Operating System	Linux	Linux Windows NT/7 Solaris
Programming Language(s)	FORTRAN 77 bash script	Java bash script
Compilers	GNU Fortran 77 (g77)	Sun Java Compiler
External Libraries & Versions	NetCDF 3.6.1 (unidata)	NetCDF-java 4.1 (unidata) HDF Java from HDFView2.3 (for Aqua AMSU-A)
Storage Required (GB)	70	900 (scaled integer format)
Time Required (hour)	50 hours for 14 satellites	60 hours for 6 satellites in parallel computation

6. Assumptions and Limitations

6.1 Algorithm Performance

There are two fundamental assumptions associated with the calibration algorithm: a) the end-to-end calibration of the instrument can be described by a quadratic calibration equation; b) post-launch information required to obtain the calibration coefficients have been correctly used.

On the first assumption, there are possibilities that the calibration equation is not a quadratic type for certain channels and sensors. Higher order terms in the calibration equations may exist. In this situation, two calibration coefficients are not sufficient to characterize the nature of instrument biases. Scene temperature dependent biases may occur since they cannot be removed by the calibration algorithm of the quadratic type (Zou et al., 2009).

Including high order terms than quadratic in the calibration equation is difficult since there is lack of information to determine the calibration coefficients for the high order terms. Depending on the applications of the radiance datasets, empirical bias correction schemes shall be carried out for the biases unresolved in the SNO calibration.

On the second assumption, the calibration coefficients are determined by minimizing inter-satellite biases including scene temperature dependency in biases, instrument temperature dependency in biases, and bias drifts. It is possible that other types of biases still exist that require introduction of more calibration coefficients or change of the current calibration coefficients. Once these unknown types of biases are discovered, further investigation of the validity of the calibration algorithm and coefficients are required.

6.2 Sensor Performance

This ATBD discusses the radiance FCDR which fundamentally relies on sensor performance. The sensor performance including radiometric noise equivalent temperature, calibration, spatial and spectral error effects have been discussed in the validation and accuracy section (Section 4). A summary of the performance is listed in Table 4-2, which is based on the assumption that geophysical effects or the targets being observed do not affect the sensor performance.

7. Future Enhancements

Possible future enhancement of the algorithm may include absolute calibration, warm target and cold target calibrations, as described in the following.

7.1 Enhancement 1: Absolute calibration

Although inter-satellite differences have been minimized by the SNO calibration, the absolute values of the MSU/AMSU multi-satellite level-1c radiances contain a nearly constant bias relative to an unknown absolute truth. This bias is estimated to be 0.5 to 1 K. This nearly constant bias does not affect the variability and trend analysis of the subsequent products developed from the FCDR. However, it affects data assimilations in reanalysis development and NWP forecasting. This bias needs to be determined in FCDR validation processes against certain reference observations, ideally SI-traceable standards. Future enhancement in this area includes development of validation plans as part of the MSU/AMSU FCDR development effort. This includes comparisons against GPS RO observations as well as observations from the Global Climate Observing System Upper-Air Network. However, because all observations feature certain errors, there is no guarantee that such comparisons will result in the absolute temperature values with required accuracies. Ultimately, community consensus references for absolute calibration need to be developed, which still remains a challenging task.

7.2 Enhancement 2: target calibrations

In the current algorithm, the side-lobe effect of the cosmic space cold target has been assumed to be a constant about 2K for both MSU and AMSU-A channels. However, this effect is a function of time and channels. Future enhancement on this area includes development of more sophisticated cold target calibration algorithms for more accurate level-1c radiance derivation.

The warm target temperature is currently assumed to be the average of available good PRT measurements. However, inhomogeneous heating of the warm target causes warm target thermal gradient; as a result, different PRT measurements on different warm target locations give different temperatures at the same time. This warm target thermal gradient problem causes warm target anomalies on short term time

scales. It is desirable to understand how this problem affects accuracies of level-1c radiance calibration. Future enhancement in this area will include development of a more sophisticated warm target calibration algorithm with thermal gradient effect incorporated and then an understanding of its impact on accuracies of level-1c radiances.

8. References

Cao, C., et al. (2004). Predicting Simultaneous Nadir Overpasses among Polar-Orbiting Meteorological Satellites for the Intersatellite Calibration of Radiometers. *Journal of Atmospheric and Oceanic Technology, 21(4)*, 537-542

Kidwell, K.B., edited, (1998). NOAA Polar Orbiter Data User's Guide, available at http://www.ncdc.noaa.gov/oa/pod-guide/ncdc/docs/podug/index.htm

Mo, T. (1996). Prelaunch calibration of the advanced microwave sounding unit-A for NOAA-K. *Microwave Theory and Techniques, IEEE Transactions on, 44(8)*, 1460-1469

Mo, T. (2006). Calibration of the Advanced Microwave Sounding Unit-A Radiometers for METOP-A, *NOAA Technical Report NESDIS 121*. Washington DC: NOAA/NESDIS/STAR

Robel, J., et al. edited, (2009). NOAA KLM user's guide, available at http://www.ncdc.noaa.gov/oa/pod-guide/ncdc/docs/klm/index.htm

Saha, S., et al. (2010). The NCEP climate forcast system reanalysis. *Bulletin of the American Meteorological Society, 91(8)*, 1015-1057

Rienecker, M. M., et al. (2011), MERRA: NASA's Modern-Era Retrospective Analysis for Research and Applications, J. Clim., 24, 3624–3648, doi:10.1175/JCLI-D-11-00015.1.

Zou, C.-Z., et al. (2009). Error structure and atmospheric temperature trends in observations from the Microwave Sounding Unit. *Journal of Climate, 22(7)*, 1661-1681

Zou, C.-Z., et al. (2006). Recalibration of microwave sounding unit for climate studies using simultaneous nadir overpasses. *Journal of Geophysical Research, 111(D19)*, D19114

Zou, C.-Z., & Wang, W. (2010). Stability of the MSU-derived atmospheric temperature trend. *Journal of Atmospheric and Oceanic Technology, 27(11)*, 1960-1971

Zou, C.-Z., & Wang, W. (2011). Intersatellite calibration of AMSU-A observations for weather and climate applications. *J. Geophys. Res., 116(D23)*, D23113